2017

# Synergism of Quercetin and Sodium Butyrate for Controlling Growth of Glioblastoma

Matthew Alan Taylor
*University of South Carolina*

# SYNERGISM OF QUERCETIN AND SODIUM BUTYRATE FOR CONTROLLING GROWTH OF GLIOBLASTOMA

by

Matthew Alan Taylor

Bachelor of Science
University of Central Florida, 2015

---

Submitted in Partial Fulfillment of the Requirements

For the Degree of Master of Science in

Biomedical Science

School of Medicine

University of South Carolina

2017

Accepted by:

Swapan Ray, Director of Thesis

Anindya Chanda, Reader

Susan Lessner, Reader

Cheryl L. Addy, Vice Provost and Dean of the Graduate School

# ACKNOWLEDGEMENTS

Faculty:

Swapan K. Ray, PhD – Research Mentor

John Fuseler, PhD – Fluorescent Microscopy

Udai Singh, PhD – Flow Cytometry

Anindya Chanda, PhD – Thesis Committee Member

Susan Lessner, PhD – Thesis Committee Member

---

Students:

Firas Khathayer – PhD Student; Ray Lab

Alex Sougiannis – PhD Student; Murphy Lab

Narayan Raghava – Undergraduate

Jacob Heuker – Undergraduate

# ABSTRACT

Glioblastoma multiforme (GBM), or simply glioblastoma, is the most common and aggressive primary brain tumor, with a prevalence of approximately 20,000 new cases per year in the United States and a 3-year survival rate of just 2%. Quercetin (QCT) is a dietary flavonoid that can be found in common foods such as red kidney beans, cilantro, and onions. Despite little evidence showing any benefits through dietary intake of QCT, various studies show its promising anti-cancer results in vitro. In glioblastoma, QCT is able to cause significant amounts of apoptosis through a variety of mechanisms. These include activation of caspase-9 and caspase-3, deactivation of matrix metalloprotease-2 (MMP-2), inhibition of heat-shock protein-27 (HSP-27) and HSP-72, and increased p53 activity. Autophagy is a natural occurring survival mechanism that is induced when cells are subjected to environmental stressors like nutrient deprivation, high heat, or hypoxia. As a result, many synergistic studies are being performed with QCT in order to find out adequate autophagy down regulation that could complement QCT for enhancing its apoptosis inducing capabilities. Synergism is the concept of two substances providing a greater affect than the sum of their individual affects. Drugs acting in synergism with each other is a promising investigative avenue for many alternative cancer treatments, including GBM.

The drugs QCT and Sodium Butyrate (NaB) were investigated under autophagic conditions in three GBM cell lines in order to test their efficacy in slowing the

growth of glioblastoma cells in-vitro due to the reduction of autophagy. The three glioblastoma cell lines tested are C6 (rat), T98G (human), and LN18 (human). The results of this study showed a marked increase in apoptosis in all three GBM cell lines, with the most occurring in T98G. Apoptosis levels were determined via Wright Staining and Annexin V/PI staining. QCT + NaB combination treatments were also found to reduce serum-starved induced autophagy in all cell lines with the most prominent occurring in T98G. QCT alone was also found to be an autophagy inhibitor at a 25 μM concentration. These results were confirmed via acridine orange staining and western blotting. QCT + NaB was also found to act in synergism to reduce poly (ADP-ribose) polymerase-1 (PARP-1), a DNA repair enzyme, and survivin, an anti-apoptotic protein, expression in C6 cells, which further confirmed the potential efficacy of QCT + NaB to be used in conjunction with conventional chemotherapeutic therapies.

TABLE OF CONTENTS

# LIST OF TABLES

# LIST OF FIGURES

# CHAPTER 1

# INTRODUCTION

Glioblastoma multiforme (GBM), also known as simply glioblastoma, is the deadliest and most aggressive malignant primary brain tumor. Typically existing as an astrocytoma, glioblastoma tumors most commonly reside in the cerebral hemispheres; however, they can emerge anywhere throughout the central nervous system. Although it accounts for only 14.9% of all primary brain cancers, it has the highest prevalence of malignancy out of any brain tumor. These tumors become more frequent with age and more commonly affect men than women. Patients diagnosed with GBM have a median survival of 14.6 months with the current standard treatments. According to the American Brain Tumor Association, children with high grade tumors have a better prognosis than adults; with a 5 year survival rate of 25%, whereas adults have a 5 year survival rate of 10%.

The most prevalent symptoms include seizures, nausea, headaches, and vomiting. Upon diagnosis, first line therapies include surgical resection in conjunction with simultaneous radiotherapy and chemotherapy. In most cases, complete surgical resection is difficult due to the undefined borders of GBM tumors. They often spread throughout the cerebral hemispheres with tentacle-like extensions, which makes total resection without the loss of essential brain functioning nearly unattainable. Standard chemotherapy utilizes Temozolomide (TMZ), which is a DNA methylating/alkylating agent that targets $O^6$ guanine residues, resulting in a cessation of growth in the G-2 phase (Sang et al., 2014). Radiation therapy has been shown to increase overall median survival times and improve quality of life (Messaoudi et al., 2015).

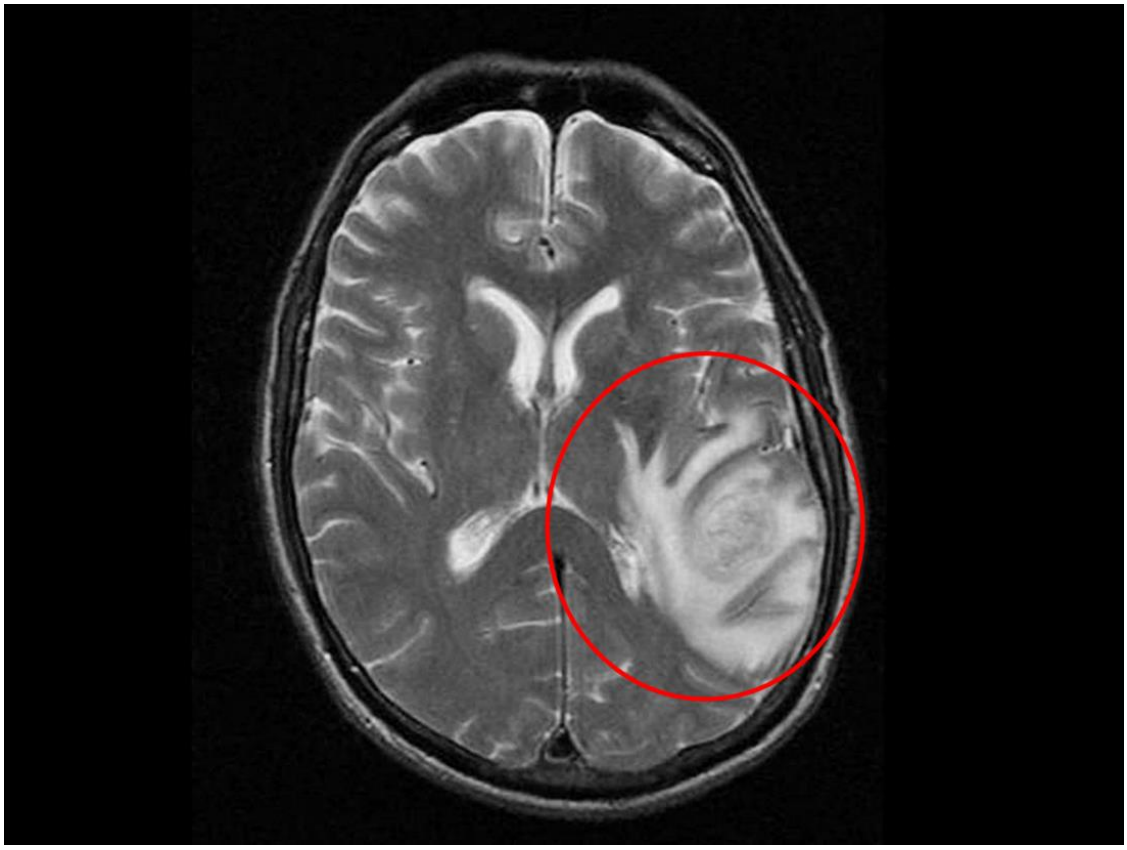

Figure 1.1: MRI image showing tentacle-like extensions of a GBM tumor located in the right hemisphere (Courtesy of Medscape).

After approximately 12 months of TMZ treatment, most GBM tumors become resistant to the tumor DNA alkylation. This occurs due to the increased activity of $O^6$-methylguanine DNA methyltransferase (MGMT) repair enzyme in GBM tumors, which leads to chemoresistant phenotypes. This mechanism, along with rapid growth and undefined borders, are the core cause of the low survival rates of GBM patients. Because of this, alternative therapies are being widely researched. The only FDA approved second-line GBM treatment is Bevacizumab, which is an antibody targeting vascular epithelial growth factor (VEGF). VEGF is highly upregulated in GBM and is responsible for glioblastoma endothelial cell proliferation (Hottinger et al., 2014). Other second-line

therapies include Cediranib, Vatalanib, Aflibercept, and Cilengitide; however, they have shown little-to-no efficacy in clinical trials.

The aim of the current study is to explore the therapeutic potential of a second-line therapy using QCT and NaB synergistically with each other. QCT is a natural bioflavonoid that is most widely known for its anti-inflammatory properties. But in recent years, QCT has proven to contain anti-cancer properties in a variety of tumors, including glioblastoma. QCT has been shown to induce apoptosis in GBM through multiple mechanisms that include activation of caspase-9 & caspase-3 and downregulation of heat shock proteins (HSP) 72 & 27 (Taylor and Ray, 2017). But despite its anti-cancer potential, QCT is not without its downsides. QCT has also been shown to alter autophagy in various GBM cell types. It was demonstrated in U373MG cells that QCT upregulated autophagy (Kim et al., 2013), whereas QCT was able to block autophagy in U87 and U251 when paired with the drug t-AUCB (Li et al., 2016). Autophagy is considered a cell survival mechanism during cancer progression. By pairing QCT with another drug, it is hypothesized that autophagy will be downregulated and apoptosis will be synergistically potentiated.

Sodium butyrate (NaB) is a well-known histone deacetylase inhibitor (HDACi) that is widely used in cancer treatment studies. Histone acetylation is important for gene expression due to acetylated lysine residues allowing a DNA strand to reside in the relaxed position. This allows for cell transcription machinery to access genes and transcribe the corresponding mRNA. The role of a histone deacetylase (HDAC) is to remove the acetyl groups from lysine residues; thus, returning the DNA into its tightly coiled form around a histone. Many cancers, including prostate, breast, and lung, have

HDAC overexpression. This results in repression of essential tumor suppressor and DNA repair genes (West and Johnstone, 2014). Over the past decade, many clinical trials have been underway to test the efficacy of HDACi in combination with standard chemo- and radiotherapies. Valproic Acid in combination with radiation therapy has been shown to be a radiosensitizer, and Vorinostat (SAHA) in combination with several chemotherapies has shown synergistic cell death (Lee et al. 2017). But despite NaB being a well-established HDACi, few studies have been performed investigating its impact on GBM. Because of its relatively unknown mechanism and the success of other HDACi drugs in combination therapy, it was determined that NaB would be the most ideal candidate for this study.

Autophagy is a cellular response triggered by environmental stressors such as high heat or nutrient starvation. In recent years, autophagy has become an area of interest in cancer research due to it serving two opposite roles in the cancer cell cycle. During tumor development autophagy is a tumor suppressive mechanism; however, during tumor progression autophagy is a pro-survival mechanism (Yang and Klionsky, 2010). This enigma opens a door to a new avenue of cancer therapy by downregulating autophagy during cancer treatment. The effect QCT has on autophagy in glioblastoma remains controversial. It has been shown to both upregulate and downregulate autophagy in different GBM cell types. The impact of NaB on autophagy has been largely undetermined. In order to develop viable cancer therapies, autophagy and its role in various types of cancer must be better understood. By investigating the synergism of QCT + NaB on GBM cells under autophagic conditions, the roles of each of these drugs and their impact on autophagy may be better understood.

# CHAPTER 2

# PROSPECTS OF ENHANCING ANTI-CANCER ACTIVITIES OF QUERCETIN IN THE TREATMENT OF GLIOBLASTOMA

Taylor, M. A., & Ray, S. K. (2017). Prospects of Enhancing Anti-Cancer Activities of Quercetin in the Treatment of Glioblastoma. *Horizons in Cancer Research, 66*, 173-192.
Reprinted here with permission of Nova Science Publishers.

## ABSTRACT

Quercetin (QCT) is a dietary flavonoid that can be found in common foods such as red kidney beans, cilantro, and onions. It is most commonly known as a neuroprotective agent; but at doses between 12.5 - 100 μM, QCT has been proven to possess potent anti-cancer activities. Despite little evidence showing any benefits through dietary intake of QCT, various studies show its promising anti-cancer results in vitro. The most common and deadly brain cancer is glioblastoma that remains incurable with any standard chemotherapy. In glioblastoma, QCT is able to cause significant amounts of apoptosis through a variety of mechanisms. These include activation of caspase-9 and caspase-3, deactivation of matrix metalloprotease-2 (MMP-2), inhibition of heat-shock protein-27 (HSP-27) and HSP-72, and increased p53 activity. In addition to induction of apoptosis, QCT upregulates autophagy in most glioblastoma cell lines. Autophagy is a naturally occurring survival mechanism that is induced when cells are subjected to environmental stressors like nutrient deprivation, high heat, or hypoxia. As a result, many synergistic studies are being performed with QCT in order to find out adequate autophagy down regulation that could complement QCT for enhancing its apoptosis inducing capabilities. The most significant hurdle to overcome with QCT treatment in glioblastoma is developing an efficient delivery method into the brain to allow its prolonged accumulation in the affected brain tissue. QCT is rapidly degraded when injected in vivo, which explains why dietary intake is unable to produce significant results. However, recent studies have shown that QCT is able to be delivered to the brain, liver, kidneys, and lungs in both mice and pig models through the use of nanoparticles. Even though much still remains undiscovered, recent advances made in blood-brain-barrier delivery systems and drug synergism have

opened a window of opportunity into future use of QCT as a viable alternative or addition to standard treatment for glioblastoma.

## 2.1 - INTRODUCTION

Glioblastoma multiforme, which is also simply called glioblastoma, is one of the most common and aggressive primary brain tumors. According to the American Brain Tumor Association, glioblastoma accounts for about 15% of all primary brain tumors with a median survival of 14.6 months from the time of diagnosis in spite of current use of surgery, radiotherapy, and chemotherapy. Standard treatment for glioblastoma includes first surgical resection followed by adjuvant chemotherapy with temozolomide (TMZ) and radiotherapy. The molecular mechanism of action of TMZ shows that it acts by methylating the $O^6$ position of guanine nucleotides in genomic DNA, resulting in cell cycle arrest and cell death (Sang et al., 2014). Recent Phase III clinical trials have shown that TMZ treatment in conjunction with radiotherapy increased median survival time from 12.1 to 14.6 months in glioblastoma patients (Hottinger et al., 2014). In most cases, the brain tumors become resistant to TMZ treatment within a year due to development of intracellular protective mechanisms such as altered DNA repair enzyme activity, p53 mutations, and overexpression of epidermal growth factor receptor (EGFR) (Haar et al., 2012; Messaoudi et al., 2015). The negligible success with the current adjuvant therapies has impelled the necessity for development of alternative treatments in order to improve the outcomes in glioblastoma patients.

Studies in our laboratory have shown that various flavonoids possess remarkable anti-cancer properties in the treatment of human glioblastoma in vitro (Das et al., 2010;

Chakrabarti and Ray, 2015a; Chakrabarti and Ray, 2015b) and also in vivo (Chakrabarti and Ray, 2016). Quercetin (QCT) is an abundant dietary flavonoid commonly found in foods such as red kidney beans, chili pepper, cranberry, onion, and tomatoes (Konar, 2013; Dajas et al., 2015). QCT has a basic flavonoid structure consisting of two separate phenolic rings A and B joined by a 3-carbon heterocyclic ring C and with all the substitutions in its rings, it is chemically called 3,3,'4,'5,7-pentahydroxyflavone (Figure 2.1). In nature, many flavonoids including QCT are bound to sugars and thus occur in O-glycoside forms due to glycosylation at any hydroxyl group of the flavonoids. The glycosylated structures of a flavonoid are the most common in nature, not the aglycone or parent molecule. The most common QCT glycoside has a sugar group at the 3-hydroxyl position, such as QCT-3-O-glucoside. QCT is highly regarded as a potent anti-oxidant that acts through its ortho-dihydroxy substitutions in its ring B and also the 2,3-unsaturation and 4-carbonyl in its ring C (Dajas et al., 2015). However, recent studies have clearly shown that QCT possesses significant anti-cancer properties. QCT acts through multiple molecular mechanisms to induce apoptosis in many types of cancers. In glioblastoma, QCT triggers the intrinsic apoptotic pathway that includes activation of caspase-9 and caspase-3 (Badziul et al., 2014), inactivation of heat-shock proteins (HSPs) (Sang et al., 2014), suppression of PI3K/Akt survival signaling (Pan et al., 2014), and inhibition of mitogen-activated protein kinase (MAPK)/extracellular signal-regulated kinase (ERK) kinase (MEK) 1 and Raf1 kinase activities (Lee et al., 2008). This multi-directional approach to induction of apoptosis gives a great potential to QCT to act as an alternative treatment for glioblastoma.

Despite the widely proven pro-apoptotic capabilities of QCT in cell culture studies, many obstacles still have to be overcome before it can be used as a viable alternative therapy for glioblastoma. The greatest challenge facing QCT therapy is its instability due to metabolic degradation in vivo. High molecular mass and low water solubility have hindered the ability of this naturally occurring dietary QCT to accumulate in the target tissues at therapeutically significant concentrations (Blasina et al., 2015). As a result, current research efforts have been focused on developing nanosomes that can be used to prevent metabolic degradation of QCT, allow penetration through the blood-brain-barrier (BBB), and maintain QCT tissue concentrations at a therapeutically effective level (Priprem et al., 2008).

Another obstacle with QCT therapy is the current understanding of autophagy and modulation of induction of autophagy by QCT. Autophagy is a cellular response to nutrient starvation and other metabolic stressors that prompt recycling of existing cytoplasmic components in order to be used as an alternative energy source (Cui et al., 2015). Present studies describe autophagy as either a pro-survival or pro-death mechanism; therefore, exact role of autophagy in cancer has been difficult to determine (Moon et al., 2015). QCT is a known up-regulator of autophagy in glioblastoma (Kim et al., 2013, Cui et al., 2015, Moon et al., 2015). The current understanding of autophagy in glioblastoma is that it acts as a pro-survival mechanism during glioblastoma progression (Kim et al., 2013). This emphasizes the need to further investigate capability of QCT to act synergistically or at least additively when combined with one of the drugs known for down regulation of autophagy.

The anti-cancer capabilities of QCT both in vitro and in vivo have been clearly demonstrated over the past decade. The high prevalence, poor prognosis, and ineffective therapies for glioblastoma have made the development of alternative therapies a significant priority. Despite the current obstacles associated with QCT, its profound therapeutic potential makes it an alternative agent that cannot be ignored. This chapter will provide a comprehensive overview of the past findings, current research, and future development paths that can be taken into consideration to use QCT as a viable alternative therapy for glioblastoma.

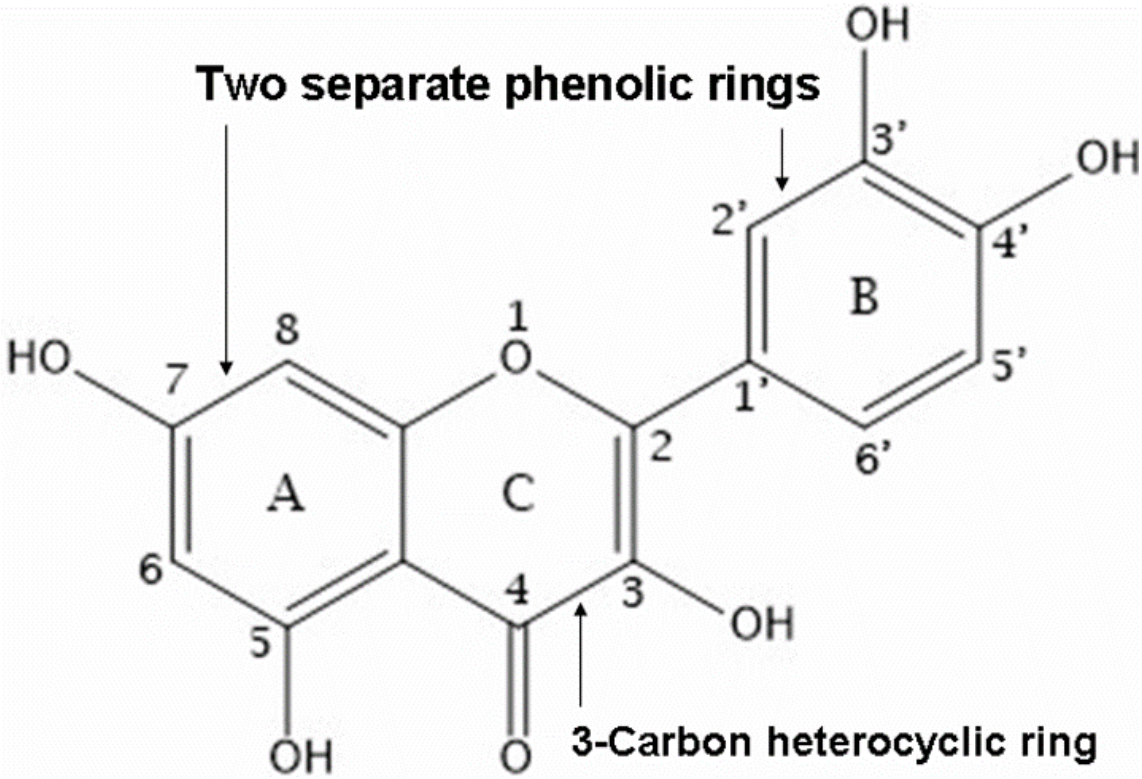


Figure 2.1: Chemical structure of QCT molecule. Its molecular formula is $C_{15}H_{10}O_7$ with a molecular mass of 302.236 and its IUPAC (International Union of Pure and Applied Chemistry) name is 2-(3,4-dihydroxyphenyl)-3,5,7-trihydoxy-4H-chromen-4-one. Chemically, it is also called 3,3,'4,'5,7-pentahydroxyflavone. This chemical structure of QCT has been established by various organic syntheses.

## 2.2 - OVERVIEW OF CURRENT TREATMENTS FOR GLIOBLASTOMA

Glioblastoma is a malignant, highly aggressive primary brain tumor that almost always carries a poor prognosis. The incidence of glioblastoma is 3 to 4 in 100,000 people per year (Hottinger et al., 2014). However, the incidence increases with age and is more common in men. According to the American Brain Tumor Association, about 3% of the childhood brain tumors diagnosed are considered as glioblastoma. Without treatment, average survival time is usually less than 1 year. With treatment median survival ranges around 14 months. Despite a poor prognosis, many patients choose to undergo surgery and standard treatment with the hopes of extending their survival as much as possible.

Upon diagnosis of glioblastoma, the first priority is the surgical resection of the tumor. Glioblastoma typically reside in the cerebral hemispheres, but tumors also have some potential to appear anywhere throughout the central nervous system. Due to the highly aggressive nature of glioblastoma, complete surgical resection is often unattainable. Without complete surgical resection, adjuvant chemotherapy or radiotherapy is a necessary next step (Hottinger et al., 2014). After surgical resection of the tumor, radiotherapy combined with simultaneous oral TMZ chemotherapy is the currently used treatment strategy. TMZ is a DNA alkylating agent that is currently the standard chemotherapy for treatment of glioblastoma. TMZ induces apoptosis by methylating $O^6$ guanine residues in genomic DNA in cancer cells, which ultimately leads to cell cycle arrest at the G2 phase (Jakubowicz-Gil et al., 2013). Standard treatments for glioblastoma patient involve a daily oral TMZ dose of 75 $mg/m^2$ of body surface area (BSA) with simultaneous radiation treatment for the first six weeks (Messaoudi et al.,

2015). This is followed by a TMZ dose of 150 - 200 mg/m$^2$ BSA for five consecutive days every 28 days. Usually within one year, glioblastoma becomes resistant to TMZ and ultimately cause recurrence of the tumor. TMZ resistance is mainly attributed to many glioblastoma cells containing $O^6$-methylguanine DNA methyltransferase, which counteracts the primary cell death mechanism of TMZ. Other resistance mechanisms include an overexpression of EGFR and p53 gene mutations (Messaoudi et al., 2015).

Due to highly aggressive nature of glioblastoma and poor outcomes of standard treatment regimen, many alternative targeted therapies are being developed. Currently the most prevalent second-line glioblastoma treatment is Bevacizumab (Bev), which is a US Food and Drug Administration (FDA) approved monoclonal antibody that targets vascular epithelial growth factor (VEGF) (Wang et al., 2016). VEGF and its variants are highly expressed in glioblastoma cells and other brain tumors (Kloepper et al., 2016). However, after multiple Phase II and Phase III clinical trials, Bev has been unable to show a consistent favorable outcome in glioblastoma patients when compared with the standard regimen of TMZ and radiotherapy (Hottinger et al., 2014). Other alternative drugs that target factors such as EGFR, BCR-Abl, PI3K/Akt, and mTOR are currently in clinical trials, but so far these drugs have shown little to no efficacy in treating glioblastoma patients.

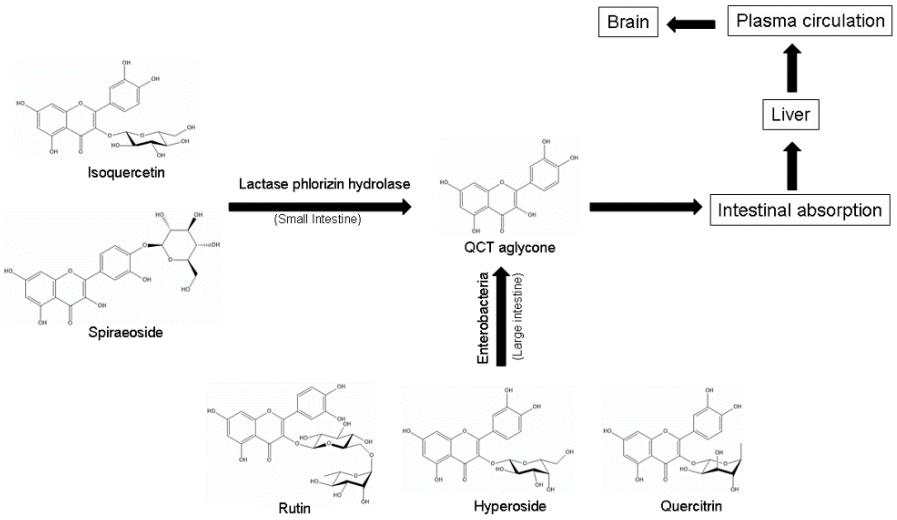


Figure 2.2: Processes and pathways for synthesis of QCT aglycone from various QCT glycosides and its biodistribution in animals. Various QCT glycosides are catabolized to QCT aglycone in small and large intestines. Absorption of QCT aglycone may ultimately transport it to some extent to the brain.

## 2.3 - QCT AGLYCONE SYNTHESIS AND BIOAVAILABILITY

QCT is one of the most common dietary flavonoids and it is found in many fruits and vegetables. In Western countries, it is estimated that an average person has an average dietary intake of 16 - 25 mg of QCT per day (Dajas et al., 2015). In vivo, QCT aglycone synthesis and its bioavailability are shown (Figure 2.2). Most of the QCT found in the diet is in its glycosylated forms, which include isoquercetin (QCT-3-O-glucoside), spiraeoside (QCT-4'-O-glucoside), rutin (QCT-3-O-rutinoside), hyperoside (QCT-3-O-galactoside), and quercitrin (QCT-3-O-rhamnoside). Once ingested, QCT glycosides are hydrolyzed by lactase phlorizin hydrolase in the small intestine and then absorbed via the sodium-dependent glucose transporter-1 (SGLT-1). After SGLT-1 mediated import, intestinal processing results in QCT glycosides for their conversion to QCT aglycone, which is considered to be the most potent anti-oxidant (Murota and Terao, 2003). QCT

aglycone is quickly processed through secondary metabolism by the liver and then distributed throughout the bloodstream (Kashino et al., 2015). QCT metabolites then attach to serum albumin in order to be circulated throughout the blood plasma. These metabolites have a half-life of 11 to 28 hours, which allow for aggressive supplementation to increase QCT plasma concentrations to high nanomolar to low micromolar range (Dajas et al., 2015). Normal dietary plasma QCT levels are typically in the low nanomolar range.

In order for QCT to be a viable treatment for glioblastoma, it must be able to pass through the BBB. A recent study performed in rats investigated the ability of dietary QCT to accumulate in the brain after heavy supplementation by either direct QCT injection or dietary intake (Ishisaka et al., 2011). The aim of this investigation was to analyze the neuroprotective effects of QCT and found that QCT was detectable in the rat brain tissue at the pmol/g level (Ishisaka et al., 2011). An earlier study determined that rats subjected to an 11-week 1% QCT diet accumulated 330 and 680 pmol/g of brain tissue (de Boer et al., 2005).

Despite the ability of QCT to penetrate the BBB and accumulate in brain tissue, no studies have shown dietary or intravenous administration of QCT aglycone or its metabolites to be a viable method for saturating brain tissue to cancer therapeutic levels. Some recent in vitro studies, however, have determined that 25 - 100 µM QCT can be an effective pro-apoptotic concentration in various glioblastoma cell lines (Kim et al., 2013; Pan et al., 2014). Therefore, it can be implied that QCT dietary supplementation is not an effective method for achieving sufficient level of QCT in vivo for treating or preventing glioblastoma.

## 2.4 - MECHANISMS OF ACTION OF QCT FOR INDUCING APOPTOSIS

Over the last decade, QCT has been shown to be a potent anti-cancer compound. In addition to its free radical scavenging properties, QCT can also induce apoptosis in glioblastoma cells while showing negligible side effects on normal tissues (Pozsgai et al., 2013). This unique property has demonstrated that QCT has the potential to be a viable second-line therapy for inducing apoptosis in human glioblastoma cells (Pan et al., 2014). Although the complete mechanism of QCT for induction of apoptosis in glioblastoma has yet to be fully discovered, QCT has been proven to act through an intrinsic multi-mechanistic pathway leading to final phase of apoptosis. The mechanisms for ultimate induction of apoptotic cell death due to QCT include down regulation of PI3K/Akt survival signaling (Pan et al., 2014), inactivation of HSP-27 and HSP-72 (Sang et al., 2014), inhibition of MAPK pathways (Lee et al., 2008), and also suppression of the JAK/STAT3 signaling pathway (Michaud-Levesque et al., 2012), and activation of caspase-9 and caspase-3 (Badziul et al., 2014) in glioblastoma cells (Figure 2.3). This type of multi-targeted mechanisms of QCT in glioblastoma may hold the key to combating the chemoresistance issue associated with TMZ treatment and also key to providing hope of improving patient outcomes.

The most prevalent mechanism of QCT for induction of apoptosis in glioblastoma is the activation of caspase-9 and caspase-3, as mentioned above. In a recent study, it has been shown that QCT in a dose dependent manner can increase activation of caspase-9 and caspase-3 (Kim et al., 2013). Maximum activation of caspase-9 occurred at 100 µM

QCT, while maximum activation of caspase-3 happened at 75 µM QCT in human glioblastoma U373MG cells (Kim et al., 2013). Caspases play a crucial role in induction of apoptosis by their contributions to apoptotic pathways that are manifested in morphological and biochemical features. Caspase-9 is considered an initiator caspase in the intrinsic mitochondrial pathway of apoptosis (McIlwain et al., 2013). After QCT acts through the intrinsic mitochondrial pathway, cytochrome c is released from mitochondria into the cytosol and then cytosolic cytochrome c is combined with Apaf-1 to form an apoptosome, which recruits pro-caspase-9 and ultimately leads to activation of caspase-9 (Badziul et al., 2014). QCT activates caspase-9 that then proceeds to activate caspase-3 by causing a conformational change to expose active sites on caspase-3 (McIlwain et al., 2013). Caspase-3 then proceeds to activate various pro-apoptotic proteins including a DNase that ultimately degrades genomic DNA causing cell death. Activation of caspase-9 and caspase-3 by QCT has been widely demonstrated both in single drug (Kim et al., 2013) and multi-drug combination (Jakubowicz-Gil et al., 2013; Badziul et al., 2014) studies.

Many other studies have also shown that QCT acts in glioblastoma cells through the inhibition of the PI3K/Akt survival pathway (Pozsgai et al., 2013). Since its discovery, the PI3K/Akt pathway has been of great interest due to its crucial role in cell survival in cancers. Many cancer types have the upregulated PI3K/Akt signaling, which may be a major contributing factor to chemoresistance (Vara et al., 2004). A recent study investigating QCT treatments alone or in combination with TMZ in two glioblastoma cell lines U-251 and DBTRG-05 demonstrated the ability of QCT to down regulate the PI3K/Akt survival signaling pathway (Pozsgai et al., 2013). QCT significantly decreased

phospho-Akt levels in glioblastoma cells both in single and TMZ combination treatments. In a more recent study, it has been demonstrated that PI3K/Akt pathway contributes to mitochondrial health by promoting anti-apoptotic Bcl-2 stabilization (Pan et al., 2014). Bcl-2 is an important oncoprotein and well-known for its role in preventing mitochondrial pathway of apoptosis in cancer cells. Down regulation of the pro-survival PI3K/Akt signaling pathway enables QCT to induce mitochondrial pathway of apoptosis in glioblastoma cells. Interestingly, QCT has also been shown to drastically increase phospho-ERK levels (Pozsgai et al., 2013), which may result in increased Bcl-2 translation. In contrast, a more recent study demonstrated that QCT in a dose dependent manner decreased phospho-ERK1 levels (Pan et al., 2015). The reason for this discrepancy has yet to be determined. Obviously, a decrease in phospho-ERK1 is highly desirable for decreasing the Bcl-2 translation.

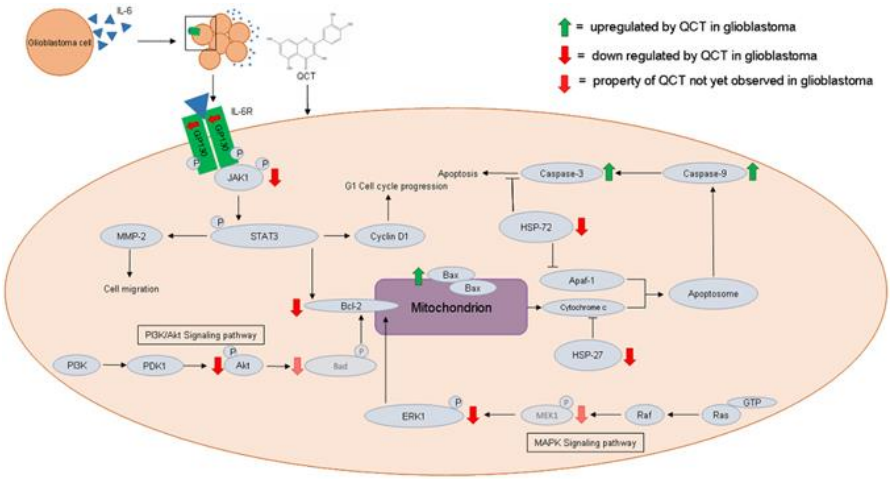


Figure 2.3: Molecular mechanisms of action of QCT for inhibition of growth and induction of apoptosis in glioblastoma cells. Various studies have confirmed the capability of QCT in down regulating cell migration, PI3K/Akt survival signaling, cell cycle progression, anti-apoptotic Bcl-2 protein, and HSPs. QCT promotes pro-apoptotic Bax homodimerization and inhibition of HSPs (HSP-27 and HSP-72) to trigger mitochondrial release of cytochrome c and facilitate formation of apoptosome, respectively, leading to activation of the intrinsic pathway of apoptosis in glioblastoma cells.

Another mechanism involved in the multi-targeted approach of QCT for induction of apoptosis in glioblastoma cells is the inactivation of the HSP-27 and HSP-72. These HSPs play very important roles in cell survival when exposed to stressful environments. In cancers, HSPs can hinder treatment by inhibiting the intrinsic mitochondrial pathway of apoptosis. HSP-27 inhibits apoptosis by binding to cytosolic cytochrome c; thus, stopping it from binding to Apaf-1 to form the apoptosome (Takayama et al., 2003). HSP-72 functions by acting on Apaf-1 and preventing Apaf-1 from binding to cytosolic cytochrome c (Badziul et al., 2014) and HSP-72 can also migrate to the nucleus to prevent nuclear DNA degradation due to caspase-3 mediated activation of a DNase (Jakubowicz-Gil et al., 2013). Indeed, QCT is considered to be one of the best HSP inhibitors and it is known to down regulate both HSP-27 and HSP-72 in glioblastoma cells (Badziul et al., 2014). The ability of QCT to inhibit HSP activity enhances its ability to induce apoptosis in glioblastoma cells through the intrinsic pathway by further down regulating anti-apoptotic factors. Due to the oncogenic nature of HSP expression in cancer cells, inhibition of their activity by QCT demonstrates a novel approach to future cancer therapies.

QCT also has the ability to inhibit the STAT3 signaling pathway in glioblastoma. The STAT3 pathway is one of the most studied signal transduction pathways due to its prevalent and potent roles in inflammation and cancer. It has been demonstrated that there is a significant correlation between STAT3 activation and tumor malignancy (Birner et al., 2010). QCT reduced glioblastoma cell growth due to inhibition of the STAT3 signaling pathway by blocking the phosphorylation of GP130 and simultaneously suppressing the JAK1 activation (Michaud-Levesque et al., 2012). In glioblastoma, the

STAT3 pathway is responsible for Bcl-2 upregulation, promoting cell migration through MMP-2 activation and cell cycle progression through cyclin D1 expression. Results showed that QCT in a dose dependent manner inhibited MMP-2 secretion in presence of IL-6. This suggests that QCT is a suitable therapy for preventing glioblastoma invasion and metastasis. It was also observed that QCT stopped cell cycle progression by inhibiting cyclin D1 expression. However, inhibition of cyclin D1 expression occurred only in presence of IL-6 (Michaud-Levesque et al., 2012). It has been demonstrated that glioblastoma cells heavily secrete IL-6 (Hong et al., 2007) and this provides an opportunity to QCT to enable its inhibitory effect on cyclin D1 expression for blocking glioblastoma cell growth.

## 2.5 - AUTOPHAGY ENIGMA IN QCT THERAPY FOR GLIOBLASTOMA

Autophagy is a cellular response to environmental stressors such as nutrient starvation, high heat, or metabolic stress. This process involves intracellular degradation of cytoplasmic components via acidic lysosomes in order to provide additional amino acids and other building blocks for essential cellular processes (Cui et al., 2015). In cancers, autophagy is an important topic because of its ability to either act as a protective mechanism or promoter of apoptosis. During cancer development, autophagy is considered to be tumor suppressive mechanism; while during cancer progression, autophagy promotes cancer cell survival (Yang and Klionsky, 2010). Most cancers are detected during their progression. It is becoming clear nowadays that novel strategies

need to be developed to make QCT get around autophagy and put forward apoptosis for slowing the progression of glioblastoma cell growth (Kim et al., 2013).

Despite the impression that autophagy pathway progresses in a simplistic manner, its physiological effects remain largely misunderstood. In vitro studies show that autophagy is most easily triggered through nutrient starvation of the cells in culture. An autophagic cell then encompasses its organelles into a specialized vesicle, termed the autophagosome. The autophagosome fuses with acidic lysosome, thereby the engulfed components are digested and the resulting amino acids and other building blocks are reused for essential cellular processes (Yang and Klionsky, 2010). Detection of autophagy is performed by measuring the amount of increase in LC3B II (which is present in the autophagosome) or the amount of decrease in sequestosome 1 (SQSTM1), also known as the ubiquitin binding protein p62 (which is a substrate for lysosomal degradation in the autophagosome), in the cell (Moon et al., 2015).

Autophagy is enigmatic in the use of many alternative and also standard chemotherapeutic agents for glioblastoma. Several studies have so far demonstrated that QCT is an up-regulator of autophagy in glioblastoma as well as in other forms of cancer cells (Kim et al., 2013; Cui et al., 2015; Moon et al., 2015). This property is one of the major pitfalls of QCT in the treatment of cancer, revealing autophagy being a cellular protection mechanism during cancer progression. A well-designed study demonstrated how QCT could induce protective autophagy in human glioblastoma U373MG cell line (Kim et al., 2013). The same study also showed that QCT was unable to induce autophagy in human glioblastoma T98G cell line. This is an example of the unique properties of each human glioblastoma cell line to a specific drug treatment, emphasizing

the need to develop therapeutic strategies that are effective in many glioblastoma cell types. Presence of protective autophagy was shown in U373MG cells by measuring the amount of decease in apoptosis in the cells following treatments with QCT alone and QCT combined with chloroquine (an anti-malarial drug known to block autophagy). The results showed that when combined with chloroquine, QCT was capable of inducing autophagy by utilizing new mechanisms. In addition to activation of caspase-9 and caspase-3, caspase-7 was also activated in apoptotic cells (Kim et al., 2013). It can be stipulated that QCT has unforeseen mechanistic approaches to induction of apoptosis that may be inhibited by autophagy. In order for QCT to be a viable therapy for glioblastoma, it must be paired with another complimentary drug for acting synergistically or additively for promoting induction of both extrinsic and intrinsic pathways of apoptosis in various glioblastoma cell types.

## 2.6 - QCT SYNERGISM FOR CONTROLLING GLIOBLASTOMA

Synergism, by definition, is the combination of two or more therapeutic agents that accentuate a greater therapeutic effect, greater than the sum of their individual effects. This is an important topic in development of successful cancer therapy because not all individual drugs are perfect for promoting apoptosis and achieving desirable therapeutic outcomes. QCT, as previously mentioned, is a known autophagy inducer in some glioblastoma cells (Kim et al., 2013), which may promote overall cell survival during glioblastoma progression. Studies suggest that pairing QCT with another compound to inhibit autophagy will heighten the therapeutic effects of QCT in glioblastoma (Kim et al., 2013).

While investigating the anti-cancer capabilities of QCT in glioblastoma, several studies were conducted to gauge which drugs might pair best with QCT. So far the most common pairing is QCT with TMZ, which is the most common chemotherapeutic drug used for treatment of glioblastoma, as demonstrated in two recent studies (Jakubowicz-Gil et al., 2013; Sang et al., 2014). Both studies emphasized the ability of QCT to inhibit activities of HSP-27 and HSP-72. One of these groups showed that HSP-27 could contribute to glioblastoma malignancy and its chemoresistance to TMZ (Sang et al., 2014). It was suggested that increased HSP-27 phosphorylation might be an indicator for TMZ chemoresistance. Their investigation also demonstrated that glioblastoma U251 and U87 cell lines were insensitive to TMZ. However, QCT in combination with TMZ was able to sensitize the glioblastoma cells to TMZ by inhibition of HSP-27 phosphorylation and an increase in caspase-3 activity. The earlier study provided a more comprehensive look at the molecular mechanisms of the treatment of combination of QCT and TMZ in T98G cells (Jakubowicz-Gil et al., 2013). Even though some studies suggest autophagy being a cell survival mechanism (Kumar et al., 2016), other studies imply that high enough levels of autophagy may eventually lead majority of the cancer cells decide to die by apoptosis (Jakubowicz-Gil et al., 2013). Both QCT and TMZ were able to induce apoptosis in T98G cells, but neither drug increased levels of autophagy (Jakubowicz-Gil et al., 2013).

Another synergistic study combined QCT and imperatorin for treatment of T98G cells to further investigate the roles of HSPs in glioblastoma tumorigenesis (Badziul et al., 2014). Imperatorin is a furanocoumarin and a phytochemical that can be used as an analgesic, anti-inflammatory, anti-coagulant, and photosensitizing agent. It is also widely

reported that imperatorin has potent anti-cancer properties. This study found that combination of 50 µM QCT and 50 µM imperatorin caused more apoptosis than when the drugs were used separately. The investigators also concluded that inhibition of HSP-27 and HSP-72 was highly crucial in sensitizing glioblastoma cells to various forms of treatment (Badziul et al., 2014).

Further study showed the consequences of the combination of QCT and sorafenib in the treatment of astrocytoma MOGGCCM cell line and glioblastoma T98G cell line (Jakubowicz-Gil et al., 2014). Sorafenib was originally developed to inhibit Raf kinase in order to treat malignant brain tumors. However, clinical trials did not yield significant therapeutic results. It was hypothesized that sorafenib in combination with QCT would produce greater therapeutic effects than with sorafenib alone. This study observed that sorafenib alone was a potent autophagy inducer in T98G cells, but not in MOGGCCM cells. When QCT was used in combination with sorafenib, synergistic amounts of apoptosis were seen in MOGGCCM cells. In the T98G cells, QCT showed little increase in amounts of apoptosis when compared with sorafenib treatment alone. When levels of expression of HSP-27 and HSP-72 were blocked by the short interfering RNA (siRNA), the most commonly used RNA interference (RNAi) technology, both tumor cell lines became increasingly more sensitive to QCT treatment (Jakubowicz-Gil et al., 2014). Thus, all the above mentioned studies demonstrate how inactivation of HSPs through QCT synergism can be a promising strategy in the development of alternative therapies for making glioblastoma cells amenable to apoptosis.

## 2.7 - QCT DELIVERY TO THE BRAIN

The most prevalent obstacle hindering the development of QCT-based glioblastoma therapy is the inability of QCT to be efficiently delivered to the brain. This issue contains two components: (1) poor bioavailability of QCT in the plasma and (2) difficulty of many compounds including QCT to penetrate the BBB. Both of these disadvantageous components are addressed by furthering the development of QCT-loaded nanocarriers. A nanocarrier is a nano-sized compound that is used to carry various compounds throughout the body. They are typically created by inserting a biologically unstable compound (e.g., QCT) into a biologically stable structure (e.g., micelles, liposomes, various polymers) (Liu et al., 2014). QCT makes an excellent candidate for utilization of nanocarriers due to its low water solubility and rapid metabolic degradation (Blasina et al., 2015).

Currently, many studies are being performed with the hopes of determining the most efficient QCT-nanocarrier that utilizes efficient delivery and provides therapeutic potency. First of all, in order for QCT to be a viable anti-cancer treatment, it must be adequately distributed to the brain tissues. A study investigating the relationship between QCT and cognition demonstrated that the intranasal administration of QCT-loaded liposomes provided more efficient brain delivery than orally administered liposomes (Priprem et al., 2008). This is due to the olfactory pathway bypassing the BBB and providing QCT direct access to the brain. A very recent study expanded on the use of lipid-based nanocarriers and their ability to deliver QCT to the brain (Kumar et al., 2016). These investigators compared the use of nano lipidic carriers (NLCs) with solid lipid nanoparticles (SLNs). NLCs utilize biocompatible compounds such as phospholipids,

tocopherol acetate, and glyceryl behenate (a monoester of glycerin and behenic acid). SLNs, on the other hand, utilize a solid lipid structure that is stabilized by various emulsifiers. This study found that the use of lipid-based nanocarriers increased the biodistribution of QCT to the brain 3.2 times (SLN) and 5.6 times (NLC) when compared with the unaltered QCT (Kumar et al., 2016).

With oral administration being the most convenient form of drug delivery for many types of medication, this route cannot be overlooked. Indeed, a recent study investigated the ability of QCT-loaded cationic liposomes to assess distribution of QCT throughout the body (Liu et al., 2014). Cationic liposomes are known to be advantageous for oral administration of a drug due to their ability to interact with negatively charged intestinal mucosa. This study found that these QCT-loaded cationic nanostructured lipid carriers (QR-CNLC) were able to prolong exposure time in the gastrointestinal tract, which subsequently improved intestinal absorption of the medication. QCT accumulated in the lung, kidney, and liver. But insignificant amounts of QCT were found in the brain tissue (Liu et al., 2014).

The next step after optimization of delivery is to ensure the therapeutic potency of the nanoparticle-delivered QCT. A group of investigators examined the ability of QCT to induce apoptosis in rat glioblastoma C6 cells in vivo following delivery of the PEG2000-DPS-coated QCT nanoparticles to the rat brains (Wang et al., 2013). They were able to conclude from their results that sustained QCT concentrations in rat brain tissues led to significant amounts of apoptosis through the induction of intrinsic pathway. They measured increase in cytosolic cytochrome c levels, which eventually led to increases in caspase-9 and caspase-9 activities (Wang et al., 2013). In addition to all these studies that

we outlined here, many more studies need to investigate efficient methods for achieving abundant biodistribution of QCT to the target tissues. Overall, significantly more research must be conducted that can bridge the gap among QCT delivery, biodistribution, and anti-cancer potential in glioblastoma *in vivo*.

## 2.8 - CONCLUSION

QCT is one of the most abundant dietary flavonoids that it is found in many fruits and vegetables. QCT and many other flavonoids are known as potent anti-oxidants. But over the past decade the anti-cancer potential of QCT has also been widely recognized. In the treatment of glioblastoma, QCT has great potential in being an alternative second-line therapy. It initiates high amounts of apoptosis in glioblastoma cells by activation of caspase-9 and caspase-3, inhibition of HSPs, and down regulation of MAPK, PI3K/Akt, and STAT3 signaling pathways. However, several hurdles must be overcome before QCT can be used as a viable therapy for glioblastoma. Our current understanding of autophagy and how it affects various cancer subtypes must be expanded. Some recent studies suggest that QCT in combination with an appropriate chemotherapeutic agent can circumvent autophagy and act synergistically to promote induction of apoptosis in different glioblastoma cells. Also an efficient in vivo QCT delivery method must be developed to penetrate BBB and sustain sufficient QCT concentrations in the brain in order to combat progression of glioblastoma growth. Despite the long road of discovery and delivery that await, we think that QCT is a promising flavonoid that in a synergistic combination has the high potentials to improve the treatment outcomes in the near future in many patients who are afflicted with glioblastoma.

# CHAPTER 3

# SYNERGISTIC EFFECT OF QUERCETIN AND SODIUM BUTYRATE IN INHIBITION OF AUTOPHAGY AND INCREASE IN APOPTOSIS IN RAT AND HUMAN GLIOBLASTOMA CELLS

## ABSTRACT

Glioblastoma is the most common and aggressive primary brain tumor, with a prevalence of approximately 20,000 new cases per year in the United States and a 3-year survival rate of just 2%. Surgery alone does not cure glioblastoma because the diffuse residual tumor cells, which are never eliminated by surgery, eventually cause recurrence of the tumor. Due to the poor prognosis and limited current treatment options for this malignant disease, new therapeutic strategies must be investigated. Nutrient deficiency and hypoxia in the tumor foster autophagy, which acts as a process of recycling of building blocks of cells to promote survival and proliferation of glioblastoma cells. Different molecular attributes contribute to prevention of apoptosis in glioblastoma cells. We explored the synergistic efficacy of quercetin (QCT) and sodium butyrate (NaB) in rat C6 as well as in human T98G and LN18 glioblastoma cell lines using Trypan Blue dye staining. The results indicated that 25 µM QCT and 1 mM NaB exhibited the greatest synergistic effect on apoptosis. The synergistic effect of QCT + NaB was measured in inhibition of autophagy in the 48-h serum-starved glioblastoma cells using acridine orange staining. We found down regulation of autophagy due to treatment with combination of drugs, when compared with a single drug. Next, the morphological feature of apoptosis was measured by Wright Staining, which showed occurrence of approximately 50% apoptosis in each cell line; with the greatest impact being on T98G. Exposure of cell membrane phospholipids, an early biochemical feature of apoptosis, was quantified via Annexin V staining and flow cytometry. We found that glioblastoma cells treated with QCT + NaB increased induction of apoptosis (between 50 and 60%), whereas the single treatment caused less induction of apoptosis (between 20 and 40%).

Our study is designed for understanding the morphological and biochemical features of inhibition of autophagy and enhancement of apoptosis in the serum-starved glioblastoma cells due to synergistic effect of QCT and NaB.

## 3.1 - INTRODUCTION

Glioblastoma Multiforme is the most common and aggressive primary brain tumor with a median survival time with treatment of 15 months. Currently there is no known cure. Modern treatments include simultaneous chemotherapy and radiotherapy with second line treatments, such as Bevacizumab, having little impact on prognosis. Since GBM has such a bleak prognosis, continued alternative therapy development is crucial. Today, two widely pursued treatment development avenues exist for GBM, immunotherapy and synergism. This study focuses on analyzing the synergism between the bioflavonoid quercetin and histone deacetylase inhibitor sodium butyrate and their effects on apoptosis and autophagy.

Drug synergism is a common therapeutic avenue to treat complicated pathologies such as hypertension, diabetes, and cancer. Many conventional chemotherapeutic agents prove to be unsuccessful in many cancer treatments due to the molecular and genetic variations in cancer subtypes, leading to eventual drug resistance (Jang et al., 2015). To combat these poor outcomes, methods such as targeted nanoparticle delivery, monoclonal antibodies, and drug synergism are actively being developed. Although finding a suitable synergistic drug combination for a certain disease has been difficult to ascertain, when that combination is found it can give a detailed mechanistic view into disease progression and drug interactions (Yin et al., 2014). Synergistic drug combinations can also provide

highly specific treatment avenues with lower overall side effects. Many chemotherapies have proven to be highly cytotoxic with unspecific cellular targets. Temozolomide (TMZ), the most common first-line chemotherapy treatment for GBM, is an orally delivered DNA alkylating agent that eventually induces GBM chemo-resistance (Winkler et al., 2014). Synergism aims to lower the overall chemotherapy drug dose by combining the therapy with a less cytotoxic drug while simultaneously increasing the anticancer effects on a patient's specific cancer subtype (Yin et al., 2014).

A 2014 clinical study conducted on GBM patients showed that TMZ administration in conjunction with chloroquine synergistically increased the chemosensitivity of GBM to TMZ by chloroquine-induced autophagy downregulation (Golden et al., 2014). Autophagy in cancer is generally considered to be a protective mechanism, but can also inhibit growth during tumor development (Yang and Klionsky, 2010). Similarly to the Golden et al. study, this study aims to study the synergism between QCT and NaB on glioblastoma by measuring its impact on apoptosis and autophagy. QCT, a known autophagy upregulator, is also a potent anti-cancer agent. NaB is a HDACi that has been shown to induce autophagy in various forms of cancer, but little investigation has been performed in GBM. More importantly, NaB has the potential to make epigenetic changes in GBM to allow QCT to further potentiate its anti-cancer effects (Yurtsever et al., 2013).

## 3.2 - MATERIALS AND METHODS

*Reagents*. Hyclone™ RPMI-1640 Medium, Hyclone™ trypsin-EDTA, phosphate buffered saline (Fisher Scientific), fetal bovine serum (BioABChem), penicillin/streptomycin (cellgro®), 0.4% trypan blue solution (Sigma Aldrich), Kwik-Diff™ Solution #1, Kwik-Diff™ Solution #2, Kwik-Diff™ Solution #3, acridine orange (Invitrogen™), Annexin V-FITC (BD Biosciences), propridium iodide (BD Biosciences), Annexin V buffer solution (BD Biosciences), caspase-3 polyclonal antibody (Santa Cruz Biotechnology), LC3B monoclonal antibody (Cell Signaling Technologies), cleaved PARP-1 monocloncal antibody (Cell Signaling Technologies), survivin monocloncal antibody (Santa Cruz Biotechnology), Bcl-2 polycloncal antibody (Santa Cruz Biotechnology), Bax polycloncal antibody (Santa Cruz Biotechnology), β-Actin polycloncal antibody (Santa Cruz Biotechnology), 4X Laemmli Sample Buffer (Bio-Rad), Clarity™ Western ECL Substrate (Bio-Rad), quercetin (Sigma Aldrich), sodium butyrate (Sigma Aldrich).

*Cell Culture.* C6 rat glioblastoma cells were provided by ATCC # CCL-107. T98G human glioblastoma cell line was provided by ATCC # CRL-1690. LN18 human glioblastoma cell line was provided by ATCC # CRL-2610. All cell lines were grown in Hyclone™ RPMI-1640 medium with 10% fetal bovine serum and 1% penicillin/streptomycin. Serum starved samples were grown in Hyclone™ RPMI-1640 medium with 0% fetal bovine serum (FBS) and 1% penicillin/streptomycin (P/S). Cells were grown in a humidified incubator at 37°C and 5% $CO_2$.

*Experimental Procedure.* Appropriate amounts of GBM cells were plated on either 100x15 mm petri dishes or 6-well suspension culture plates according to each

experimental protocol. Samples were grown for 24 hours in RPMI-1640 medium containing 10% FBS and 1% P/S for 24 hours to allow cell adhesion and recovery to occur. Samples were then serum starved for 24 hours with RPMI-1640 medium containing 0% FBS and 1% P/S for 24 hours in order to induce autophagy. Samples were then treated for 24 hours with either 25 µM QCT, 1 mM NaB, or a combination of 25 µM QCT + 1 mM NaB. Control samples were grown in replenished serum-starve medium (RPMI-1640 w/ 0% FBS + 1% P/S). Samples were then tested with the appropriate experimental protocols.

Figure 3.1: A visualization of the cell culture protocol for all experiments conducted throughout the study.

*Statistical Analysis.* All experiments were performed with a minimum of $n \geq 3$. Standard error was calculated with the equation: *Standard Error* = *StDev*($n_1$,$n_2$,..$n_x$)/*Sqrt*($n$). Only upward error bars were used because the lower error bars are assumed. Statistical significance was calculated via One-way ANOVA and p-values were calculated by a Fisher post-hoc test with the Minitab Express software.

## Trypan Blue Exclusion Assay

The first step in this study is to determine the cell viability for each GBM cell line at varying doses of both QCT and NaB. In order to do this, a trypan blue exclusion assay (TBEA) was performed. Trypan blue is a diazo dye characterized by its impermeability to viable cells. It is used in clinical settings by opthamologists during anterior segment

surgeries such as corneal transplants (Jhanji et al., 2011). Laboratory testing for cell viability is just as profound. TBEA for cell viability uses the premise that dead or dying cells lose their membrane integrity, which allows the dye to infiltrate the cells. The samples can then be read under a microscope and counted in order to determine cell viability by using the formula:

$$\textit{Viable cells (\%)} = 100 - (\textit{\# of apoptotic cells} \div \textit{total \# of cells} \times 100)$$

Despite its simplicity and short experimetal timeframe, TBEA has two caveats (Strober, 1997). This test assumes that every cell with a permeable membrane is apoptotic, which is sometimes not the case (Cooper & McNeil, 2015). Another issue is that data collection relies on the precision and accuracy of manual experimenter quantification . But despite these downfalls, TBEA is a simple, reliable, and efficient method for determining cell viability.

The TBEA was used in order to calculate synergism. Synergism is when two separate compounds produce an effect that is greater than the sum of their individual effects. This concept identified the most ideal doses of QCT and NaB to be determined in order to clearly demonstrate the impact of the interaction of these two drugs on GBM cells. Cell viability data was inputted into the program CompuSyn (ComboSyn, Paramus, NJ) to calculate the combination index (CI) value of QCT and NaB at varying dosages. A CI value is a concept developed by Paul Talalay and Ting-Chao Chou in 1984 that aims to quantify synergism. They developed an equation called the *median-effect equation* that utilizes concepts from the Henderson-Hasselbalch equation, Hill equation, Michaelis-Menten equation, and Scatchard equation to normalize dose-effect

values to quantify synergism (Chou, 2010). The mathmatical formulas for calculating synergism is as follows:

$$f_a/f_u = (D/D_m)^m$$

*Median-Effect Equation*

$$D_x = D_m[f_a/(1-f_a)]^{1/m} \rightarrow CI = \sum_{j=1}^{n} \frac{(D)j}{(Dx)j}$$

*D = Dose, $f_a$ = fraction affected, $f_u$ = fraction unaffected, $D_m$ = median-effect dose, m = slope or kinetic order*

A CI value less than 1 indicates synergism, with doses being more synergistic as their CI value approaches zero. CI values greater than 1 indicate antagonism, which means the combined drugs are working against each other. A CI value equal to 1 indicates the drugs are additive (Chou, 2010). The doses used were QCT 12.5 µM, QCT 25 µM, QCT 50 µM, QCT 100 µM, NaB 1 mM, NaB 3 mM, NaB 5 mM, NaB 8 mM, and combinations of each single dose.

GBM cell lines C6, T98G, and LN18 were grown and treated using the previously described experimental protocol. The samples were harvested via trypsinization for two minutes. Trypsin was neutralized by adding 1 ml RPMI-1640 10% FBS 1% P/S medium to 0.5 ml trypsin. Samples were spun at 3000 RPM for 4 minutes and washed twice with 1X phosphate buffered saline (PBS). One part cell suspension (10µl) was mixed with one part 0.4% trypan blue (10µl) for 3-5 minutes at room temperature. Then 10µl of cell + trypan blue mixture was added to a hemocytometer and read at a 10X magnification. Samples were counted and calculated according to the previously described equation and plotted on Microsoft Excel 2016.

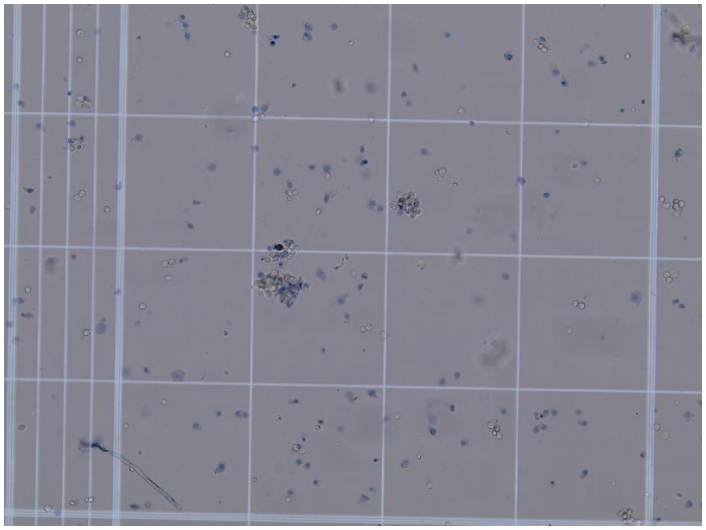

Figure 3.2: Trypan blue exclusion assay with T98G cells drugged with QCT 25 µM + NaB 1 mM visualized at 10X on a hemocytometer using an Olympus BX53 microscope.

**Wright Stain**

Wright staining was used to visualize the morphological signs of apoptosis in GBM cells. The technique is more commonly used to stain peripheral blood smears and bone marrow, but adequately stains most types of cells. Eosin dyes are used in histology to stain cytoplasmic components such as amino acids and proteins. Methylene blue is a basic thiazine dye that is able to stain astrocytic nuclei purple. Wright Staining uses a combination of eosin (red) and methylene blue dyes to give a multi-dimensional picture of cell morphology (Yue, 2014).

This technique was utilized to visualize the morphological changes that occur when GBM cells are underoging apoptosis. The most prevalent change that occurs to apoptotic cells is condensation and fragmentation of the nucleus. One of the greatest hallmarks in the apoptosis molecular pathway is the caspase activation cascade. After the apoptosome is formed through the intrinsic mitochondrial apoptosis pathway, caspase-9 activates caspase-3 (Taylor and Ray, 2017). Caspase-3 activation then causes cleavage of nuclear structural proteins, such as lamin, which promps the degredation of the nucleus

structure. Early apoptosis shows the nucleus forming a crescent shape, followed by complete nuclear condensation in the later stages of apoptosis. It is important to note that cell membrane integrity is still in tact. This is a process called *karyorrhexis* (Ziegler & Groscurth, 2004).

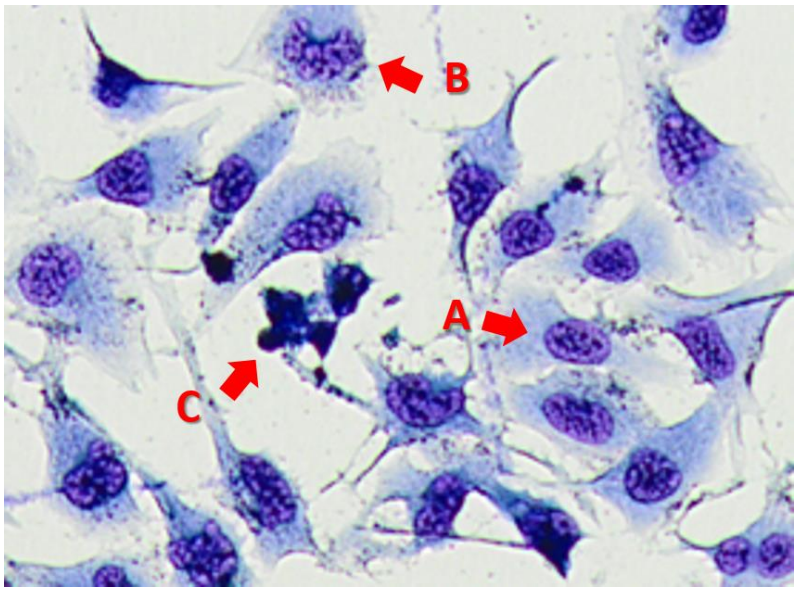


Figure 3.3: Wright staining of T98G GBM cells dosed with QCT 25 µM + NaB 1 mM. (A) A normal, non-apoptotic cell (B) Cell undergoing early apoptosis showing a crescent shaped nucleus (C) Late apoptotic cells showing complete nuclear condensation and cell shrinkage.

Another morphological sign of apoptosis is cellular membrane degredation and blebbing. Blebbing is a protrusion of the cell membrane caused by degredation of membrane structural proteins such as actin and β-catenin; along with gelsolin, Gas2, and PAK2, which help maintain organization and attachment of the cytoskeleton. Due to membrane degredation, the cell will begin to lose volume during the middle to late apoptotic stages. Blebbing will occur due to the increased pressure of the cytoplasm caused by the membrane shrinkage. Decreased membrane integrity will allow protrusions of cytoplasm to appear (Ziegler and Groscurth, 2004).

As blebs begin to separate, nuclear fragmentation will start to initiate. These fragments have lost membrane integrity and will expose intracellular contents to the external environment. Under most circumstances, these intracellular components will be phagocytosed; thus, not causing an inflammatory response (Ziegler and Groscurth, 2004). Phagocytosis is initiated by the externalization of phosphatidylserine, which is a glycerophospholipid that resides on the internal side of the cellular membrane. Upon initiation of apoptosis, the enzyme flippase in inactivated which allows for the externalization of phosphatidylserine (Verhoven et al., 1995). Phosphatidylserine signals macrophages to phagocytose the apoptotic cells. If apoptotic cells are not phagocytosed by the host immune system, their degradation patterns will begin to resemble necrosis.

Necrosis is a form of cell death that does not undergo the normal apoptosis mechanism. It is often initiated by factors such as high heat or a toxic environment. Morphologically the greatest difference between apoptosis and necrosis is necrotic cells lose membrane integrity in the very early stages of cell death. Necrotic cells can be distinguished by massive swelling of the cell, caused by polar molecules passing through the porous cell membrane. Necrotic cells are often not quantified when measuring amounts of apoptosis in a sample due to it being a form a cell death not caused by the desired drug treatments (Ziegler and Groscurth, 2004).

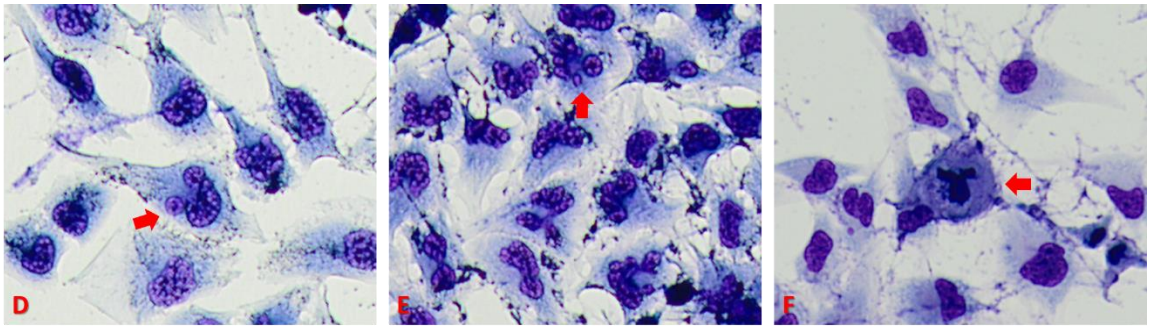


Figure 3.4: Image D shows cell membrane blebbing in T98G GBM cells treated with a 24 hour dose of QCT 25 µM. Image E shows nuclear fragmentation in T98G GBM cells treated with a 24 hour dose of NaB 1 mM. Image F shows necrosis in T98G GBM cells in a 48 hour serum-starved control sample.

Approximately 100,000-300,000 C6, T98G, and LN18 GBM cells were grown in preparation for wright staining using the previously mentioned experimental protocol in 6-well plates. Upon sample readiness, treated RPMI-1640, 0% fetal bovine serum (FBS), 1% penicillin/streptomycin (P/S) medium is removed by a Pasteur pipette with careful consideration taken to not aspirate free-floating cells. Immediately after medium removal, 1 ml of Kwik-Diff™ Solution #1 is added to each well for 25 seconds in order to fixate the cells to the plates. Solution #1 is removed by a Pasteur pipette and 1 ml Kwik-Diff™ Solution #2 is added to each well for approximately 20 seconds. Solution #2 is removed via Pasteur pipette and approximately 0.7 ml Kwik-Diff™ Solution #3 is added to each well for approximately 20 seconds and then removed with a Pasteur pipette. Samples are then washed with 1 ml $dH_2O$ to remove any excess dye. The samples are immediately read on an Olympus BX53 microscope at 10X magnification. Images were taken using an Olympus SC30 camera mounted on the BX53 microscope. Apoptosis was quantified by manually counting approximately 300 cells, differentiating between apoptotic and non-apoptotic. Apoptotic cells were characterized by the previous described criteria. Percentage of apoptosis in each sample was calculated by:

*Percent Apoptosis (%) = [# of Apoptotic Cells ÷ Total # of cells] x 100*

These results were then plotted in Microsoft Excel 2016. Each experiment was performed in triplicate.

**Annexin V**

A common and efficient way to quantify apoptosis in a cell population is the Annexin V test. It utilizes a dual Annexin V-FITC + Propidium Iodide (PI) stain to determine the physiological state of samples undergoing a form of cell death. Annexin V is a $Ca^{2+}$ dependent phospholipid binding protein that has a high affinity to phosphatidylserine, a cellular membrane phospholipid that becomes externalized in the early stages of apoptosis. PI is a fluorescent dye that is unable to permeate viable cell membranes. It is commonly used in flow cytometry of fluorescent microscopy to evaluate whether a cell is live, apoptotic, or necrotic. A combination of both Annexin V-FITC and PI paints a clear picture of the stages of cell viability in a sample population (Hingorani et al., 2011).

A flow cytometer is a powerful tool that is used to measure many different properties of a cell population. It is based off the premise of shooting a laser at an individual cell, then analyzing the resulting light scatter patterns. Flow cytometers have the ability to measure any property of a cell, as long as the fluorescent probes are conjugated to bind to the desired property. This versatility allows flow cytometers to measure anything from DNA, RNA, cytoplasmic acidity, membrane permeability, various proteins, receptors, and many more. In addition, multiple fluorescent probes can be analyzed simultaneously on the same cell. This allows for precise categorization of individual cells into a maximum of 4 subpopulations displayed on a biaxal graph.

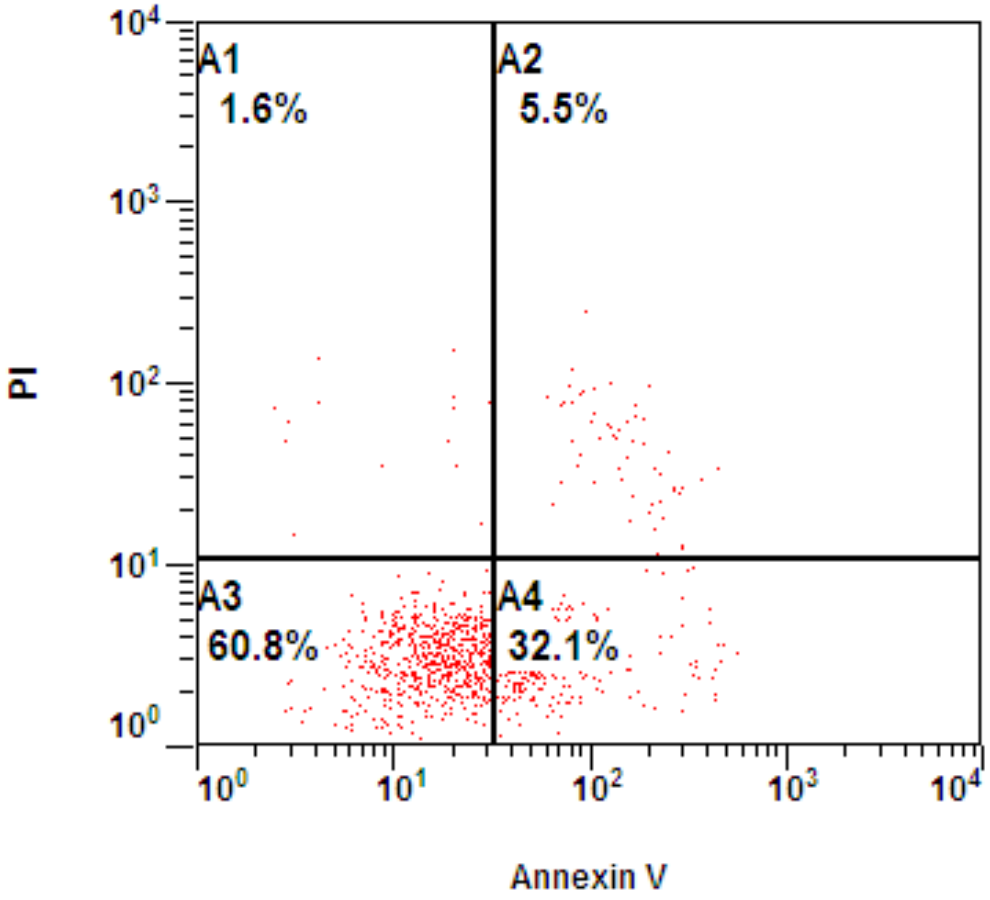


Figure 3.5: This is a flow cytometry graph of C6 cells treated for 24 hours under 48 hour serum starvation with QCT 25 µM + NaB 1 mM. The graph is divided into 4 subpopulations: A1 = AnnexinV$^-$/PI$^+$, A2 = AnnexinV$^+$/PI$^+$, A3 = AnnexinV$^-$/PI$^-$, A4 = Annexin V$^+$/PI$^-$. Each graph represents 10,000 cells.

These four subpopulations display cells in different physiological states. Quadrant A3 represents AnnexinV$^-$/PI$^-$, which means neither Annexin V or PI dyes bound to or penetrated the cell. This indicates that phosphatidylserine has not been externalized and the cell membrane is fully intact; thus, determining that the cells are fully viable. Quadrant A4 represents AnnexinV$^+$/PI$^-$ cells, which means Annexin V is bound to those cells, but PI was unable to penetrate the cell membrane. This indicates

that the cells are undergoing the early stages of apoptosis. Quadrant A1 shows cell populations that are AnnexinV$^{-}$/PI$^{+}$, meaning that PI was able to penetrate the cell membrane, but Annexin V did not bind to the cell. This subpopulation shows cells that were mechanically damaged, usually caused by experimenter error when handling the samples. Quadrant A3 represents cells that are AnnexinV$^{+}$/PI$^{+}$, meaning that both Annexin V bound to the cell and PI was able to penetrate the deteriorating membrane. The cells in this subpopulation are either necrotic, in the late stages of apoptosis, or dead. Since both necrotic cells and late apoptotic cells are able to bind Annexin V and PI, differentiating them in this subpopulation is not possible.

When performing the Annexin V test, all samples were grown and treated according to the previously described experimental protocol. Approximately 500,000 cells were grown in 6-well plates for 24 hours before serum starvation and treatment began. At the time of collection, samples were stained according to the BD Biosciences standard protocol. Treated RPMI-1640 medium, 0% FBS, 1% P/S was removed from each 6-well plate. 500 µl of 1X trypsin was added to each plate for 3 minutes in order to reduce cell adhesion. The trypsin was then neutralized with 1 ml RPMI-1640, 10% FBS, 1% P/S medium and the cells were gently pipetted into 1.5 ml microcentrifuge tubes. Samples were spun at 3,000 RPM for 4 minutes. Trypsin + RPMI-1640 was removed from the samples via Pasteur pipette and each sample was washed with 200 µl Annexin V binding buffer. The 200 µl Annexin V binding buffer was removed via Pasteur pipette and replaced with fresh 100 µl Annexin V binding buffer. The cells were then evenly distributed throughout the binding buffer by gentle pipetting. 5 µl Annexin V-FITC and 5 µl PI was added to each sample, and incubated in the dark at RT for 15 minutes. After

the incubation has completed, 400 µl Annexin V binding buffer was added to each sample. The samples were then transferred to flow cytometry tubes for analysis.

In order to configure the Cytomics FC 500 Flow Cytometer to read each cell line accurately, three control samples were prepared: (1) Blank sample – untreated 48 hr serum-starved cells + 500 µl Annexin V binding buffer (2) FITC – untreated 48 hr serum-starved cells + 500 µl Annexin V binding buffer + 5 µl Annexin V-FITC (3) PI – untreated 48 hr + 500 µl Annexin V binding buffer + 5 µl PI. These sample measurements allowed for specific quadrant setup according to the properties of each cell line. Graphs were generated with PI staining on the Y-axis and Annexin V-FITC on the X-axis.

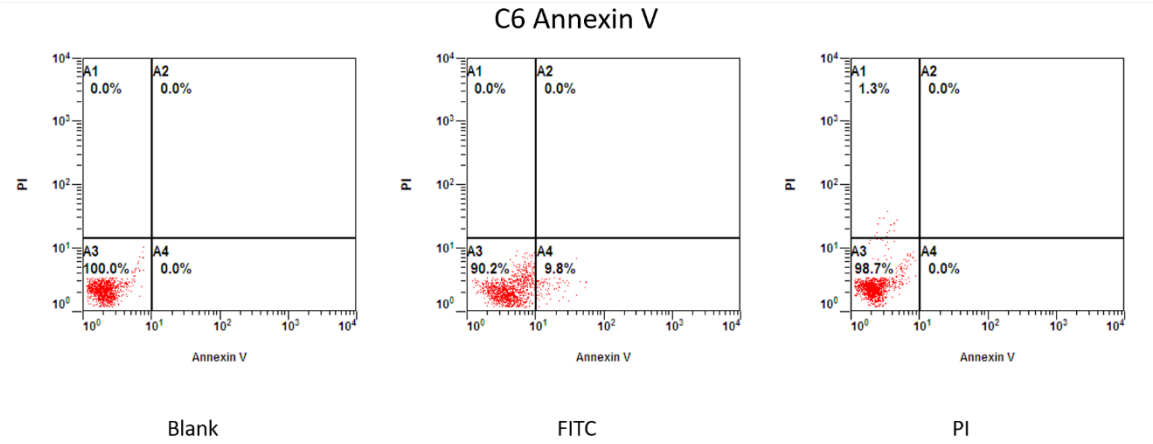


Figure 3.6: The three loading controls used to set up the quadrants and compensation for C6 Annexin V. The C6 GBM cells shown here are untreated and serum starved for 48 hours. Quadrants were drawn based on the populations of cells from each stain.

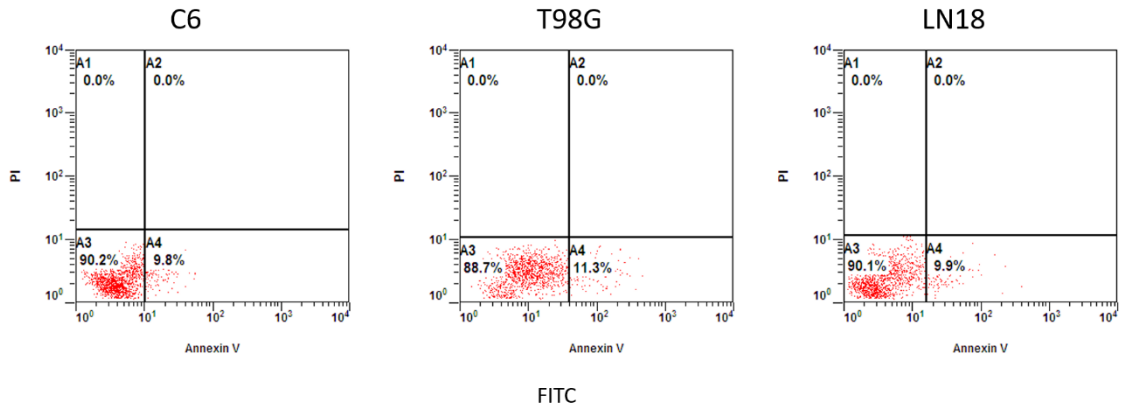


Figure 3.7: This figure depicts untreated 48 hr serum starved FITC-only stained C6, T98G, and LN18 cell measurements in the Cytomics FC 500 Flow Cytometer.

The vertical division between quadrants A1 & A2 and A3 & A4 was determined by two criteria. Firstly, the line was drawn at the division between the viable and early apoptotic cell populations. But in many samples, the division between both populations was not well defined. Therefore, the second criteria is based off the data collected with trypan blue and Wright Staining. Those tests showed approximately 10% apoptosis in all control samples under 48 hour serum starvation across all cell lines. In staying consistent with that trend, the vertical quadrant line was drawn in accordance to the previously measured basal levels of apoptosis.

The horizontal quadrant line remained fairly consistent across all cell lines. The AnnexinV$^{-}$/PI$^{+}$ cells had a more clearly defined border than the AnnexinV$^{+}$/PI$^{-}$ cells. This may be due to early apoptotic cells having variable amounts of phosphatidylserine externalized, which would cause cells to increase steadily across the X-axis with less clearly defined population borders. Mechanically damaged cells would continue to allow similar amounts of PI to penetrate the membrane until the cell becomes completely saturated, thereby generating a more well-defined population border.

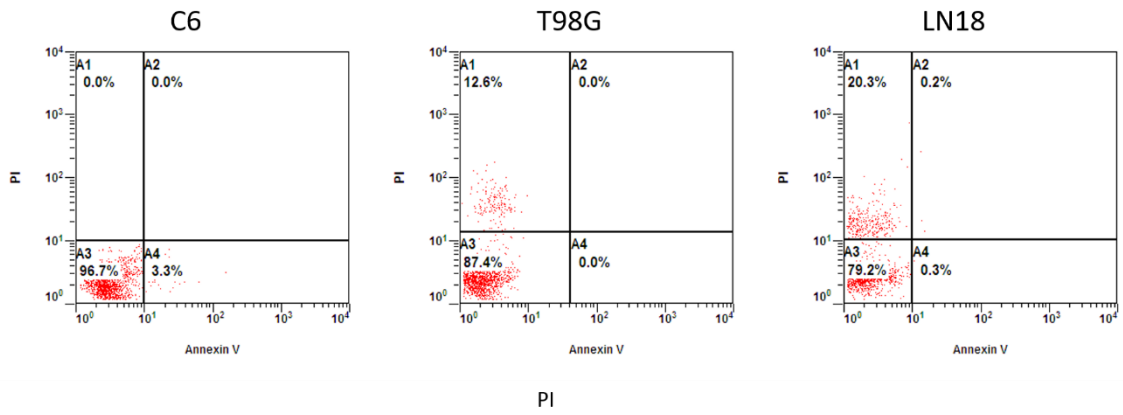


Figure 3.8: Flow cytometry data showing C6, T98G, and LN18 untreated cells under 48 hr serum starvation. This is demonstrating the clearly defined borders of AnnexinV$^-$/PI$^+$ cells compared to AnnexinV$^+$/PI$^-$ cells in figure 3.1.

## Acridine Orange

Acridine orange (AO) staining is a multi-faceted approach to visualize variations in the cell cycle. AO is a basic cell-permeable dye that has been widely used in cytochemistry by staining DNA and RNA (Thomé et al., 2016). It binds to dsDNA through intercalation and binds to ssDNA/ssRNA through electrostatic interactions. Under a fluorescent microscope, AO emits green fluorescence at 530 nm and red fluorescence at 640 nm (Lauretti et al., 2003). Another common application for AO dye is visualization of acidic vesicular organelles (AVO) produced by autophagy. AO is able to penetrate the cells and emit a bright red fluorescence when interacting with a high $H^+$ environment. Since the basic AO dye is protonated when exposed to low pH, it is unable to cross the cell membrane and exit the cell (Pierzynska-Mach et al., 2014).

Autophagy is a cellular process characterized by the formation of autophagosomes. Autophagosomes are formed during microautophagy, where parts of the cytosol and mitochondria are engulfed and eventually linked with an autolysosome to eventually be degraded. Autophagy is considered an essential cellular process that

maintains a baseline level of activity in order to recycle old organelles and initiate protein turnover. However, autophagy also acts as a cellular protection mechanism when cells are exposed to stressful environments such as high heat, oxidative stress, and many drug treatments (Yang and Klionsky, 2010).

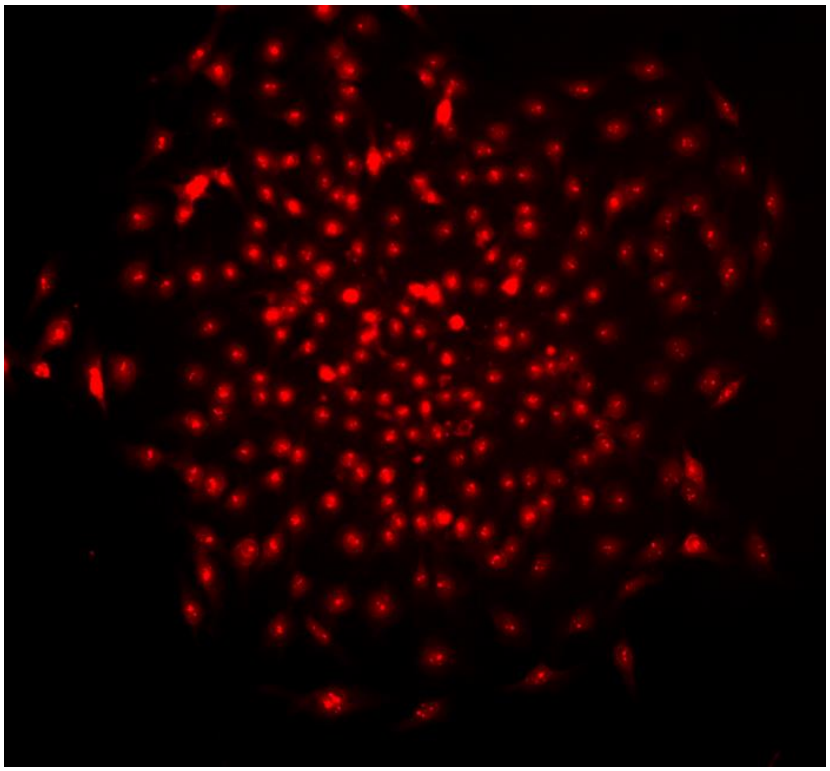

Figure 3.9: Acridine Orange staining performed on C6 GBM cells under normal growing conditions with RPMI-1640, FBS 10%, P/S 1% medium. Bright-red fluorescent cells are showing the presence of AVOs formed by autophagy at 20X magnification. Cells in the center of the cell-cluster have a higher incidence of stress-induced autophagy due to inherent nutrient starvation, while cells on the outside of the cluster show basal-levels of autophagy caused by routine cell maintenance.

In cancer research, autophagy has been a rigorously investigated topic due to its inherent cellular protection properties during cancer progression. Figure 3.9 demonstrates how cells residing in the center of a tumor become autophagic due to environmental stressors caused by the high density of cells. Many anti-cancer drugs, including QCT, are well-known autophagy upregulators. These factors contributing to

the increased autophagy in cancer cell populations can hinder the ability for many anti-cancer treatments. This concept prompted the investigation of autophagy in conjunction with the apoptotic properties of QCT + NaB in GBM.

## AO Fluorescence Microscopy

Acridine orange was used to visualize autophagy in C6, T98G, and LN18 cell populations. Cells were grown in 6-well plates with microscope coverslips placed inside each well. Approximately $1x10^6$ cells were plated onto each coverslip and the cells were grown for 24 hours in RPMI-1640, 10% FBS, 1% P/S in 37°C, 5% $CO_2$ conditions. Once the samples were ready for analysis, the medium was removed via Pasteur pipette, taking careful consideration to not aspirate any samples. The cells were then fixed with methanol for 20 seconds in order to ensure adherence to the coverslips. The cells were then washed with 1 ml 1X PBS two times. AO dye was added to each well at a concentration of 1 µg/ml and incubated at 37°C for 15 minutes. AO stain was then removed from the wells and the coverslips were placed on glass microscope slides. The samples were visualized on the LeicaDM 2500 fluorescent microscope with a Texas Red filter. All samples were photographed at 20X and 40X. The data figures were generated using 40X photos to better visualize individual cell AVOs.

## AO Flow Cytometry

It is common practice to use acridine orange with a flow cytometer to quantify autophagy. A 2011 study described acridine orange stained AVOs show bright red fluorescence (650 nm) in the FL-3 channel on a flow cytometer (Mohan et al., 2011).

Using this concept, autophagy was quantified by using a Cytomics FC 500 Flow Cytometer. Since the quantity of AVOs increases along the FL-3 axis and the amount of AVOs correlate with the amount of autophagy in a population, then the quantity of cells in FL-3 directly measured the level of autophagy in a sample. First, cells were grown according to the previously mentioned experimental protocol in 6-well plates. At the time of collection, treated medium was removed and replaced with 500 µl trypsin. The trypsin was then neutralized with 1 ml RPMI-1640 10% FBS 1% P/S medium. Cells were gently collected into 1.5 ml microcentrifuge tubes and centrifuged at 3,000 RPM for 4 minutes. The trypsin + RPMI was removed with a Pasteur pipette and washed once with 1X Annexin V Binding Buffer. The 1X Annexin V Binding Buffer was removed and 200 µl 1 µg/ml AO dye was added to each microcentrifuge tube. The cells were incubated for 15 minutes at room temperature. The AO dye was then removed and replaced with 500 ml 1X Annexin V Binding Buffer. The samples were then transferred to flow cytometry tubes and measured on the FC 500 Flow Cytometer. To quantify the amount of AVOs present in each sample, the density of FL-3 was measured. Measured samples included serum starved populations: (A) 0 hours (B) 12 hours (C) 24 hours, and also included Control, QCT, NaB, and QCT + NaB. All samples were normalized to the baseline measurement taken at 0 hour serum starvation. In theory, these samples should have the lowest amount of autophagy amongst every sample due to them being grown in

ideal conditions.

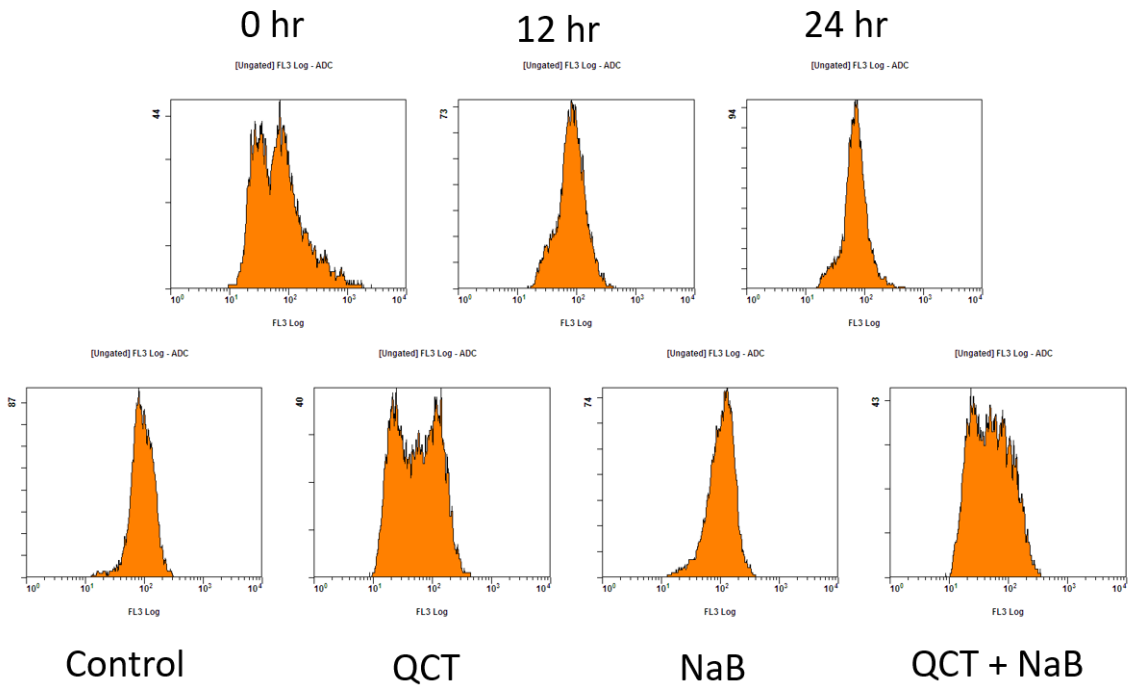


Figure 3.10: A plot of FL-3 on a FC 500 Flow Cytometer on T98G cells. 0 hr samples represents cells that have not been exposed to serum starvation; therefore, should be showing the basal level of autophagy for that cell line.

The data was originally graphed on a histogram showing the distribution of cells on the FL-3 channel. That histogram also displayed a number correlating with that density. That number, however, should not be mistaken for the percentage of autophagic cells. All cells go through a minimal amount of autophagy as a part of routine cellular maintenance (Yang & Klionsky, 2010). Therefore, just because a cell contains an AVO, does not mean they are completely autophagic. Because of this, cells grown in ideal 10% FBS conditions (0 hr) were considered to have 0% autophagy. All samples were then normalized to the 0 hr samples. Each sample was conducted in triplicate and the averages of all three samples were used to form a mean. Standard error was then

calculated with the equation: *StDev(Samples)/Sqrt(3)*. This number was used to make the upper error bar on the bar graphs made in Microsoft Excel 2016.

## Western Blotting

Western blotting is the most commonly used technique used to visualize various proteins in a cell population. It utilizes a multi-step antibody binding process that allows for specific binding and visualization for individual proteins. This method allows for the molecular pathway for apoptosis induced by QCT + NaB in GBM to be uncovered.

Samples were grown according to the previously described experimental protocol. Approximately $2x10^6$ cells were plated onto 100x15 mm petri dishes and grown for 24-48 hours. T98G and LN18 cells were grown for 48 hours to ensure adequate cell adhesion and recovery, while C6 was only grown for 24 hours due to its rapid growth rate.

*Sample Preparation:* When the samples were ready for collection, they were washed with 1.5 ml cold PBS and scraped into 1.5 ml microcentrifuge tubes. The samples were then spun at 10,000 RPM for 5 minutes. Then 200 µl RIPA lysis buffer was added to each tube. The samples were vortexed for 15 seconds and left on ice for 20 minutes to ensure complete cell lysis. The tubes were then centrifuged again at 10,000 RPM for 5 minutes and 200 µl supernatant was removed and placed into new 1.5 ml microcentrifuge tubes.

*Protein Normalization:* The importance of protein normalization is to ensure that equal quantities of protein are loaded into each well. A samples of 2 mg/ml BSA was diluted into the concentrations: 2 mg/ml, 1mg/ml, 500 µg/ml, 250 µg/ml, 125 µg/ml, 62.5

µg/ml, 31 µg/ml, 16 µg/ml. 2 µl of each diluted sample of BSA and 2 µl of each sample were added to the wells of a 96-well plate according to the following template:

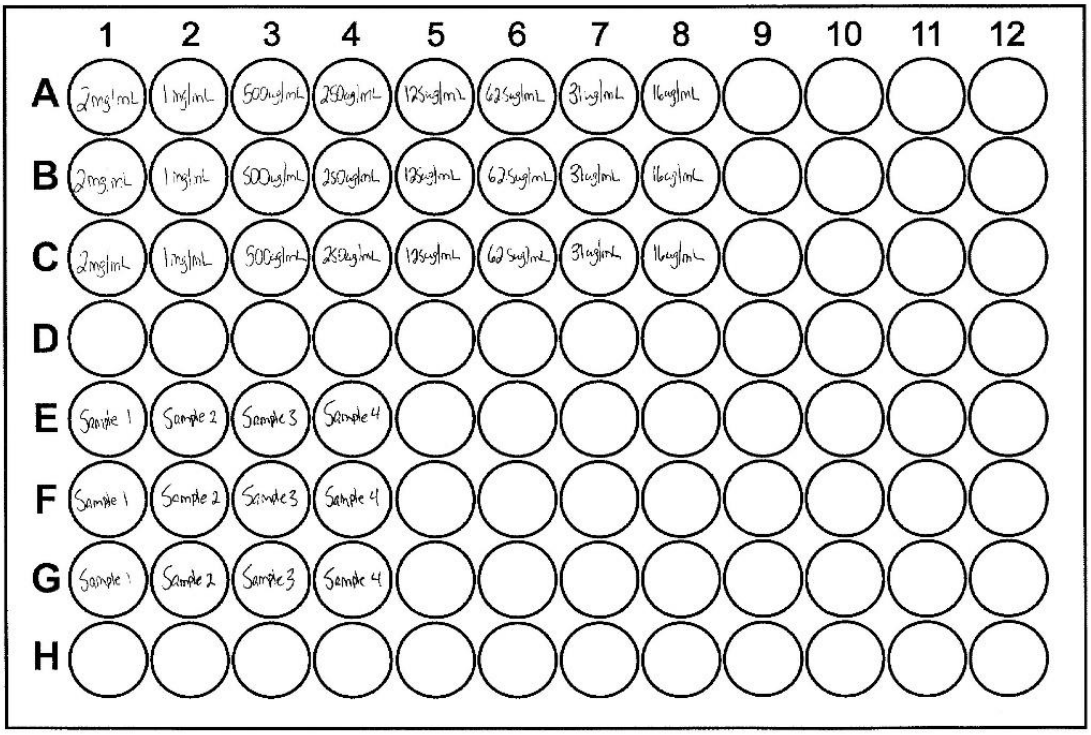


Figure 3.11: A schematic showing the layout of the 96-well plates used to normalize western blot samples.

The BSA standards and samples were then stained with 200 µl Coomassie Plus™ Protein Assay Reagent. When in contact with protein, the Bradford reagent stains blue and can be read at 595 nm to determine the quantity of protein in a sample. After waiting 5 minutes, the 96-well plate was read on a BioTek µQuant spectrophotometer at 595 nm. The results were then used to calculate the total amount of 4X Laemmli Buffer, β-mercaptoethanol (β-ME), and sample should be added to each gel electrophoresis well.

The calculations were completed as follows:

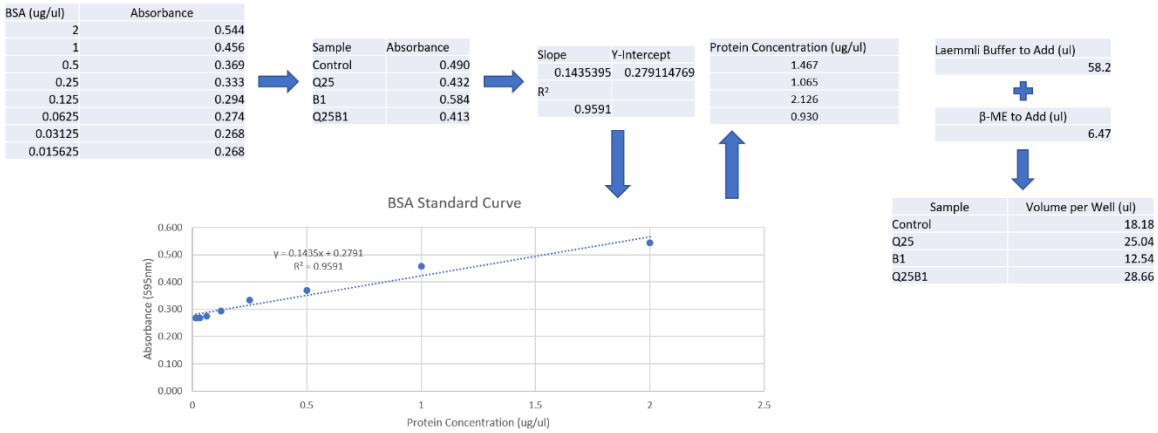


Figure 3.12: A representation of the mathematical process behind normalizing the Western Blot protein samples.

By measuring the absorbance of each known concentration of protein, a standard curve can be formed. This standard curve allows for the calculation any protein concentration based off its absorbance. The absorbances of each sample are also measured and plugged into the y=mx+b equation given by the standard curve. This calculation gives the protein concentration in µg/ul. The samples were then diluted in 3:1 Sample:4X Laemmli buffer + β-Me. The purpose of the Laemmli buffer + β-Me is to denature all proteins and give them an overall negative charge, reduce intra and inter-molecular disulfide bonds, and visualize the proteins as they are loaded and run through the SDS-PAGE gel. The samples were then heated at 95°C in a water bath for 12 minutes. At this point the samples were either loaded onto a gel or stored at -20°C for up to 6 months. When the samples were ready to be loaded onto the gel, sample volumes were calculated so 20 µl of protein was in each well.

*SDS-PAGE:* The samples were then run a through Sodium Dodecyl Sulfate Polyacrylamide Gel Electrophoresis (SDS-PAGE) gel in order to separate the sample

proteins based off size. The theory behind SDS-PAGE is that all samples have been denatured, thereby elimiating the protein tertiary structure. The sample loading buffer has also given all proteins the same negative charge. The purpose behind these property changes is to eliminate all variables between the proteins besides size. The protein samples were then inserted into 4-20% Mini-PROTEAN® TGX™ Precast Protein Gels from Bio-Rad according to the previously calculated sample-specific volumes in order to maintain the 20 µg of protein per well standard. The gels were then run at 120 V in a custom made running buffer until the bottom band of Laemmli buffer reached the end of the gel.

*Western Blotting:* After the SDS-PAGE gels were completed, the gels were transferred onto a Millipore PVDF membrane via wet transfer on the Bio-Rad Mini-PROTEAN® Tetra System. The membranes were either transferred overnight at RT with 59 mA or transferred in 1 hr at 4°C at 90 V. In order to verify that all proteins were transferred from the gel to the membrane, a Ponceau S stain was performed, then immediately washed with Phosphate Buffered Saline + .01% Tween-20 (PBST) until the red bands were removed. The membrane was then cut according to the size of the protein of interest. The membrane was then blocked with 1X PBST + 5% milk for 1 hour. This ensures that the antibodies do not bind anywhere on the PVDF membrane except their target antigen. The blocking buffer was then discarded and the membrane washed 1X with PBST. The primary antibody, which was diluted in PBST + 5% milk, was added to the PVDF membrane and incubated at 4°C overnight. The purpose of the primary antibody is to bind to the protein of interest. Primary antibodies are grown in an animal (e.g. rabbit, mouse) and made to conjugate to a specific protein (e.g. caspase-3). Slower

primary antibody incubation ensures more precise binding to the target protein, as opposed to room temperature incubation for a shorter time. The next day, the primary antibody is removed and stored at -20°C, and the membrane was washed 5x with PBST for 5 minutes per wash. After adequate washing, the secondary antibody was added to the membrane for 30 minutes. The purpose of the secondary antibody is to bind to all antibodies belonging to a certain animal and be conjugated with a flourochrome such as horseradish peroxidase (HRP). For example, if a rabbit anti-caspase-3 antibody was used as the primary antibody, then a goat anti-rabbit secondary antibody must be used. All primary antibodies were made with a dilution of 1:1,000 while all secondary antibodies were made with a 1:10,000 dilution. After 30 minutes, the secondary antibody was removed and the membrane was washed 5x with PBST for 5 minutes per wash. The next step is to add Clarity™ Western ECL Substrate, containing a peroxide solution and luminol/enhancer solution. Equal quantities of these solutions were added to the membrane and incubated at room temperature for 5 minutes. This binds to the HRP and produces a light signature that can be visualized with x-ray film. After 5 minutes the membranes were exposed to USA Scientific Blue Autoradiography & Western Blotting Film for 10 seconds – 15 minutes, depending on the light intensity of the sample. The films were then developed and scanned on a Epson Perfection V500 Photo Scanner.

Table 3.1 - Western Blotting Buffers

| 1X Running Buffer | 1X Transfer Buffer |
|---|---|
| 1) Tris – 3 g<br>2) Glycine – 14.4 g<br>3) SDS – 1 g<br>4) $dH_2O$ – fill to 1 L | 1) Tris – 3 g<br>2) Glycine – 14.4 g<br>3) Methanol – 200 ml<br>4) $dH_2O$ – fill to 1 L |

Table 3.1: A table showing the ingredients going into the custom-made western blot buffers.

## 3.3 - Results & Discussion

### Trypan Blue

Trypan blue staining was performed on C6 cells to find the most synergistic drug combination, which is represented by the lowest CI value. Only C6 was used when determining the CI value because the next stage of experimentation would include using QCT and NaB in a rat model; therefore, having the most synergistic drug combination for a rat model was the most desired. Further experimentation was done with Wright Staining and trypan blue staining to ensure that T98G and LN18 cells acted in similar ways to C6 in terms of the amount of apoptosis induced with each drug combination.

The data showed that QCT 25 µM + NaB 1 mM had the greatest amount of synergism with a CI value of 0.1746 (Table 3.2). The combination that had the next highest amount of synergism was QCT 25 µM + NaB 3 mM with a CI value of 0.2056 (Table 3.2). This alludes that the data is meaningful to the point where our chosen dosage is in the correct range. QCT was shown to have the greatest impact on apoptosis, while NaB had little effect. This conclusion is also supported with the apoptosis data collected from Wright Staining. As the concentration of QCT increased, the QCT + NaB combination became less synergistic. QCT 100 µM samples had CI values ranging from 0.38409 – 0.736, indicating that NaB was unable to act in a meaningful manner with such high QCT concentrations.

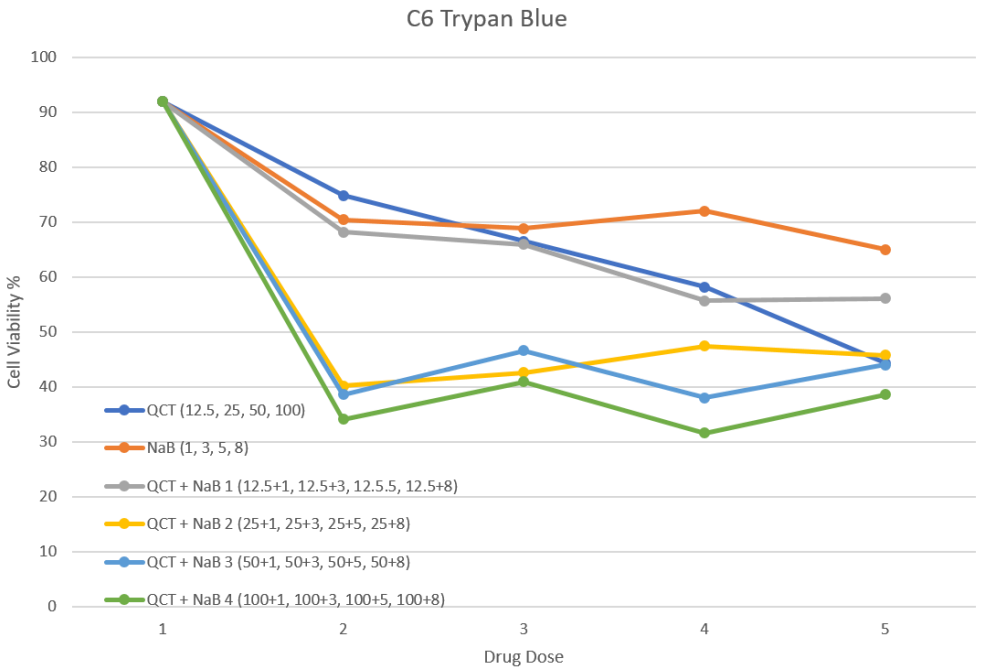


Figure 3.13: A line graph displaying the cell viability results from trypan blue staining on C6 GBM cells. This data was used to determine the most synergistic drug combination between QCT and NaB. QCT concentrations ranged from 12.5 µM – 100 µM. NaB concentrations ranged from 1 mM to 8 mM. The cell viability values were then entered into the CompuSyn software and the CI values were calculated. QCT 25 µM + NaB 1 mM was the combination found to be the most synergistic.

The greatest benefit to this technique is the low cost and ease of use. However, this technique also contains some downfalls that must be taken into consideration when interpreting this data. Unlike most experiments shown in this study, trypan blue only uses one criteria to quantify apoptosis. It relies on the premise that membrane permeability = apoptosis. But the Annexin V staining showed that membrane permeability does not necessarily mean apoptosis. Necrotic and mechanically damanged cells can also lose membrane integrity. This leads to the assumption that the trypan blue cell viability data may be slightly higher than both Wright Staining and Annexin V data. This test is also unable to determine whether or not drug treatments are cytotoxic and

causing cell death through necrosis, rather than apoptosis, which is an unwanted trait in a drug treatment.

Table 3.2 - C6 Trypan Blue Data

| | Percent Apoptosis | | | Mean | Standard Error | Cell Viability | CI Values |
|---|---|---|---|---|---|---|---|
| | Trial 1 | Trial 2 | Trial 3 | | | | |
| Control | 6.25 | 6.59 | 11.34 | 8.06 | 1.64 | 91.94 | |
| QCT 12.5 | 26.25 | 19.28 | 30.00 | 25.18 | 3.14 | 74.82 | |
| QCT 25 | 35.87 | 33.79 | 30.85 | 33.50 | 1.46 | 66.50 | |
| QCT 50 | 49.68 | 43.38 | 32.38 | 41.81 | 5.05 | 58.19 | |
| QCT 100 | 56.18 | 51.89 | 58.95 | 55.67 | 2.05 | 44.33 | |
| NaB 1 | 29.60 | 23.76 | 35.27 | 29.54 | 3.32 | 70.46 | |
| NaB 3 | 27.13 | 31.65 | 34.72 | 31.17 | 2.20 | 68.83 | |
| NaB 5 | 26.92 | 31.37 | 25.70 | 28.00 | 1.72 | 72.00 | |
| NaB 8 | 36.05 | 39.08 | 29.75 | 34.96 | 2.75 | 65.04 | |
| QCT 12.5 + NaB 1 | 34.03 | 28.80 | 32.59 | 31.81 | 1.56 | 68.19 | 0.7352 |
| QCT 12.5 + NaB 3 | 34.78 | 37.37 | 29.93 | 34.03 | 2.18 | 65.97 | 0.61563 |
| QCT 12.5 + NaB 5 | 44.12 | 43.68 | 45.21 | 44.33 | 0.45 | 55.67 | 0.24034 |
| QCT 12.5 + NaB 8 | 41.46 | 46.30 | 43.94 | 43.90 | 1.40 | 56.10 | 0.24789 |
| QCT 25 + NaB 1 | 62.38 | 59.70 | 57.46 | 59.85 | 1.42 | 40.15 | 0.17466 |
| QCT 25 + NaB 3 | 67.86 | 53.23 | 51.09 | 57.39 | 5.27 | 42.61 | 0.20564 |
| QCT 25 + NaB 5 | 49.61 | 54.44 | 53.69 | 52.58 | 1.50 | 47.42 | 0.28126 |
| QCT 25 + NaB 8 | 49.14 | 59.81 | 53.78 | 54.24 | 3.09 | 45.76 | 0.25261 |
| QCT 50 + NaB 1 | 62.57 | 62.02 | 59.65 | 61.41 | 0.90 | 38.59 | 0.31443 |
| QCT 50 + NaB 3 | 57.02 | 47.42 | 55.77 | 53.41 | 3.01 | 46.59 | 0.53313 |
| QCT 50 + NaB 5 | 57.45 | 62.44 | 66.15 | 62.01 | 2.52 | 37.99 | 0.30183 |
| QCT 50 + NaB 8 | 51.28 | 56.22 | 60.51 | 56.00 | 2.67 | 44.00 | 0.45054 |
| QCT 100 + NaB 1 | 65.66 | 64.35 | 67.57 | 65.86 | 0.93 | 34.14 | 0.46129 |
| QCT 100 + NaB 3 | 68.13 | 51.75 | 57.34 | 59.07 | 4.81 | 40.93 | 0.736 |
| QCT 100 + NaB 5 | 64.96 | 55.37 | 84.78 | 68.37 | 8.66 | 31.63 | 0.38409 |
| QCT 100 + NaB 8 | 61.76 | 56.34 | 66.04 | 61.38 | 2.81 | 38.62 | 0.63014 |

Table 3.2: This table shows the data obtained from C6 trypan blue staining. The mean was calculated by averaging the apoptosis percentage from trials 1-3. Standard error was calculated with the equation: *Stdev(Trials1-3)/Sqrt(3)*. Cell viability was calculated with the equation: *Cell viability % = 100-Mean*. CI values were calculated using the CompuSyn software. The green highlighted cell shows the lowest CI value, indicating that QCT 25 µM + NaB 1 mM is the most synergistic drug combination in C6 GBM cells.

## Wright Stain

In situ Wright Staining of C6, T98G, and LN18 GBM cell lines painted a detailed picture of the cell morphology differences between drug treatments on each cell line. In C6, apoptosis was characterized by general cell shrinkage and degradation of the glial cell protrusions. In the 25 µM QCT treatment groups, the mean apoptosis was 26.7% with a standard error of 0.7%. The 1 mM NaB treatment groups had a mean apoptosis amount of 24.0% with a standard error of 2.1%. The QCT + NaB treatment groups had a

mean apoptosis of 49.2% with a standard error of 2.9%. These results showed approximately a 95% increase in apoptosis in QCT + NaB treatment groups compared to QCT and NaB single treatment groups. Wright Staining was also able to demonstrate that C6 cell density became greatly reduced as drug treatments progressed. C6 is a rapidly growing rat GBM cell line, with a tendency to form large clusters before complete confluence is achieved. When treated with QCT + NaB, the total amount of C6 cell clusters greatly decreased. This may be due to the degradation of the extracellular matrix proteins responsible for cell adhesion and migration such as vitronectin, laminin, and fibronectin (Eroglu, 2009). The C6 cell clusters would un-adhere from each other and become free-floating in the growth medium; thus, not being detected by Wright Staining.

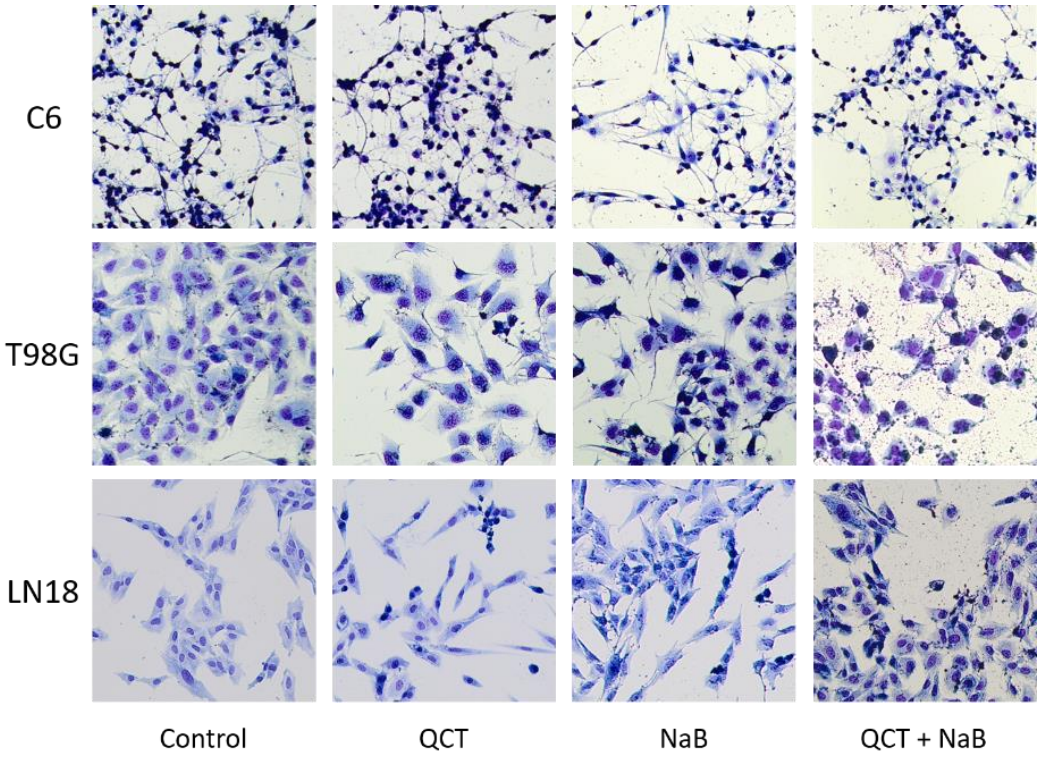


Figure 3.14: C6, T98G, and LN18 GBM cells visualized by in situ Wright Staining under 48-hour serum starvation. Samples were treated with either RPMI-1640, 0% FBS, 1% P/S Control, QCT 25 µM, NaB 1 mM, QCT 25 µM + NaB 1 mM. All images were taken under 10X magnification with an Olympus BX53 microscope.

The T98G GBM cells had the greatest amount of apoptosis across all drug dosages, as measured by Wright Staining. T98G control groups showed a basal level of apoptosis averaging at 8.4% with a standard error of 1.2%. QCT single treatment groups had a mean apoptosis of 34.4% with a standard error of 2.7%. NaB single treatment groups had a mean apoptosis of 25.4% with a standard error of 1.2%. QCT + NaB treatment groups had a mean apoptosis of 51% with a standard error of 2.4%. These results showed a synergistic increase in apoptosis of 48% and 100% from QCT and NaB groups to QCT + NaB groups, respectively. Control samples were characterized by large cell bodies and wide astrocytic protrusions. In QCT treatment groups, apoptosis was characterized by nuclear condensation, cell shrinkage, nuclear fragmentation, and membrane blebbing. Both single QCT and NaB treatment groups had these cell characterizations. However, QCT + NaB treatment groups had significant cell lysis, as seen by the copious amounts of cell debris surrounding the cell colonies.

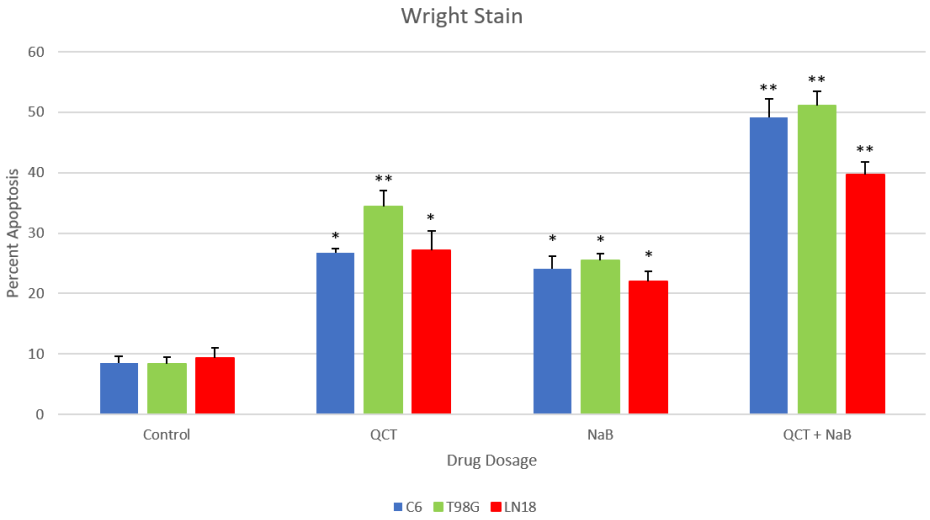


* $p < 0.05$, ** $p < 0.0001$

Figure 3.15: A graphical representation of apoptotic cells measured by Wright Staining. This graph was generated in Microsoft Excel 2016.

The LN18 showed a significant increase in apoptosis aswell, but was overall characterized as the least impacted by the dual QCT + NaB drug treatments. Control samples showed a basal level of apoptosis of 9.34% with a standard error of 1.71%. QCT treatment groups showed an average apoptosis of 27.16% with a standard deviation of 3.16%. NaB treatment groups showed an average level of apoptosis at 22.02% with a standard deviation of 1.73%. QCT + NaB treatment groups showed an average level of apoptosis at 39.69% with a standard deviation of 2.01%. LN18 control samples are characterized by an overall smaller structure than T98G. LN18 resembles epithelial cells, while T98G resembles larger brain fibroblasts. Apoptotic LN18 was identified mainly by nuclear condensation and cell shrinkage. QCT + NaB samples had detectable amounts of cellular debris, which indicated cell lysis. But these amounts were significantly less than the QCT + NaB T98G samples.

Table 3.3 - Wright Stain Data

| | Percent Apoptosis | | | Mean | Standard Error | Cell Viability |
|---|---|---|---|---|---|---|
| **C6 Wright Stain** | Trial 1 | Trial 2 | Trial 3 | | | |
| Control | 10.29 | 8.92 | 6.34 | 8.52 | 1.16 | 91.48 |
| QCT | 27.18 | 27.60 | 25.25 | 26.68 | 0.72 | 73.32 |
| NaB | 21.21 | 22.64 | 28.29 | 24.05 | 2.16 | 75.95 |
| QCT + NaB | 54.78 | 48.04 | 44.79 | 49.20 | 2.94 | 50.80 |
| **T98G Wright Stain** | Percent Apoptosis | | | Mean | Standard Error | Cell Viability |
| | Trial 1 | Trial 2 | Trial 3 | | | |
| Control | 10.13 | 8.78 | 6.15 | 8.36 | 1.17 | 91.64 |
| QCT | 29.76 | 34.51 | 38.98 | 34.42 | 2.66 | 65.58 |
| NaB | 24.32 | 27.80 | 24.19 | 25.44 | 1.18 | 74.56 |
| QCT + NaB | 47.74 | 55.73 | 49.70 | 51.06 | 2.40 | 48.94 |
| **LN18 Wright Stain** | Percent Apoptosis | | | Mean | Standard Error | Cell Viability |
| | Trial 1 | Trial 2 | Trial 3 | | | |
| Control | 5.94 | 10.76 | 11.32 | 9.34 | 1.71 | 90.66 |
| QCT | 24.59 | 33.44 | 23.44 | 27.16 | 3.16 | 72.84 |
| NaB | 18.55 | 23.66 | 23.84 | 22.02 | 1.73 | 77.98 |
| QCT + NaB | 37.01 | 38.44 | 43.63 | 39.69 | 2.01 | 60.31 |

Table 3.3: This is a numerical representation of the quantified levels of apoptosis measured via Wright Staining. All numbers were calculated with the formula: %Apoptosis = (#Apoptotic/Total Cells)*100. Between 200-300 cells were counted per dose per trial.

The main downfall of the quantification of apoptosis with Wright Staining is the subjective nature of the test. Due to the many morphological signs of apoptosis and each cell-type having unique characteristics, the counted number of apoptotic cells may vary between individuals. The main purpose of Wright Staining is to visualize the morphological changes that occur under various drug treatments. Quantifying apoptosis relative to the control can also act in a supplementary manner to Annexin V apoptosis quantification.

**Annexin V**

Annexin V/PI analysis on C6, T98G, and LN18 GBM cells yielded apoptosis vs necrosis data based off phosphatidylserine externalization and membrane integrity. C6 GBM cells showed the lowest basal level of apoptosis at 9.1% with a standard error of 1.09%. Having C6 be the cell line with the lowest amount of Control-apoptosis was expected due to the rapidly proliferating nature of C6. QCT-only samples showed a mean apoptosis of 32.2% with a standard error of 3.0%. NaB-only samples showed a mean apoptosis of 22.0% with a standard error of 0.35%. QCT 25 µM proved to be approximately 46% more potent on C6 cells than NaB, which is reinforced by the data obtained by Wright Staining. QCT + NaB samples showed a mean level of apoptosis of 39.5% with a standard error of 3.5%. Compared to the control sample, QCT + NaB samples had a 77% increase in apoptosis. However, QCT compared to QCT + NaB samples only had an 18.4% increase in apoptosis.

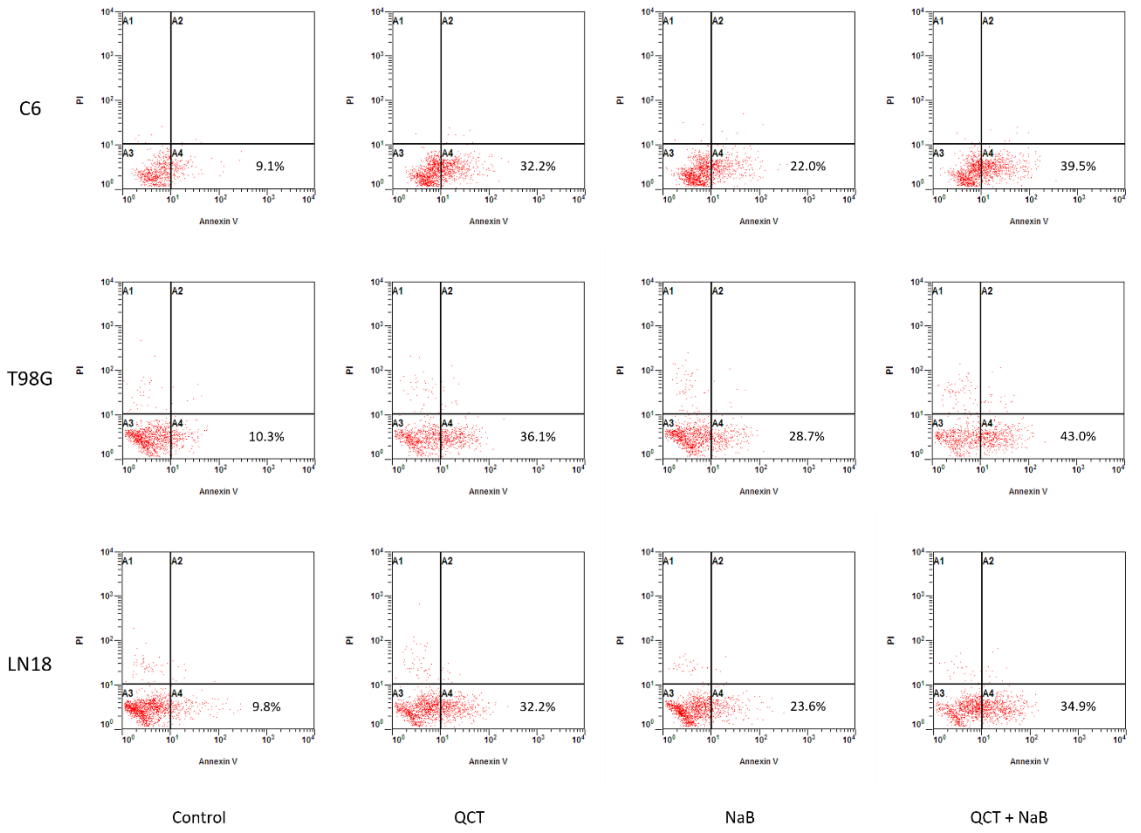


Figure 3.16: Flow cytometry dot plots generated by CXP Cytometer software by Beckman Coulter. Quadrant A1 represents $FITC^-/PI^+$ cells showing mechanical damage. Quadrant A2 represents $FITC^+/PI^+$ cells showing late apoptosis. Quadrant A3 represents $FITC^-/PI^-$ cells showing full viability. Quadrant A4 represents $FITC^+/PI^-$ cells showing early apoptosis. Percentages shown are the averages of all trials for each sample.

T98G control samples showed a slight increase in basal apoptosis compared to C6, at an average of 10.3% with a standard error of 0.58%. QCT-only samples showed significant increase in apoptosis with a mean of 36.1% and a standard error of 3.6%. NaB-only samples had a mean apoptosis of 28.7% with a standard error of 1.9%. QCT had a greater impact on T98G cells compared to NaB by about 20.5%. QCT + NaB samples had a mean apoptosis amount of 43.0%, which is the highest amount out of C6, T98G, and LN18 GBM cell lines. Compared to the control samples, QCT + NaB had a 76% increase in apoptosis, which is similar to the C6 samples. But QCT compared to

QCT + NaB samples showed only a 16% increase in apoptosis, compared to C6 samples having an 18.4% increase in apoptosis.

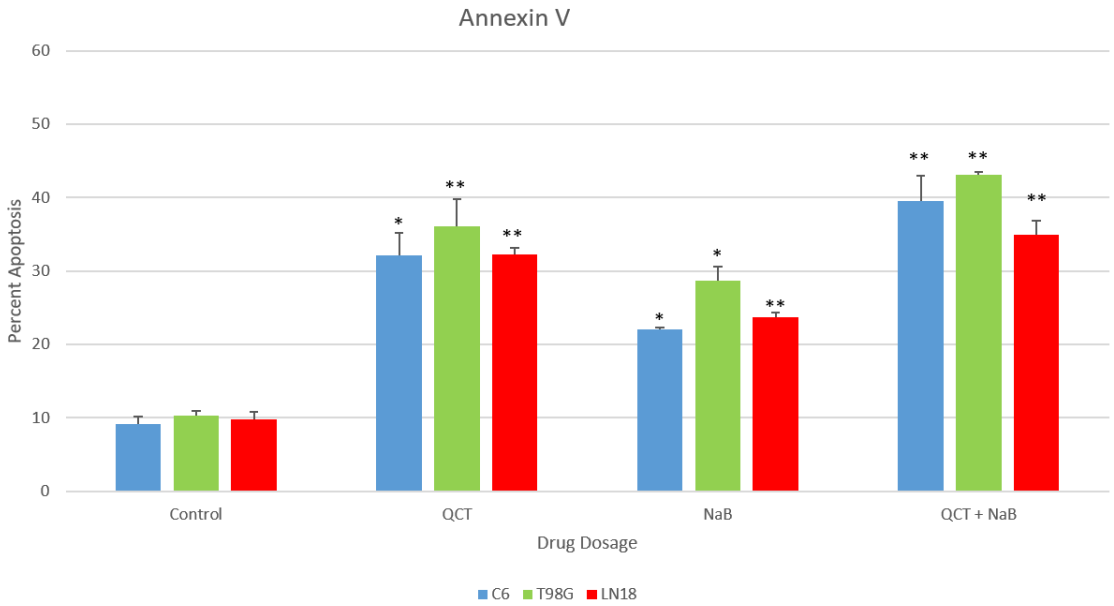


$* p < 0.05, ** p < 0.0001$

Figure 3.17: Annexin V data visualization made in Microsoft Excel 2016. Data was analyzed via one-way ANOVA followed by a Fisher post-hoc test for statistical significance.

LN18 control samples had a mean apoptosis of 9.8% with a standard error of 1.0%. QCT-only samples had a mean apoptosis of 32.2% with a standard error of 0.94%. These results were very similar to the C6 QCT-only levels of apoptosis of 32.2%. NaB-only samples had a mean apoptosis level of 23.6% with a standard error of 0.66%. These measurements were also similar to the C6-NaB samples of 22%. QCT + NaB samples had a mean apoptosis of 34.9% with a standard error of 2.0%. LN18 had the least overall apoptosis with the QCT + NaB drug combination. But despite LN18 having the lowest effect from the QCT + NaB combination treatment, it still had a 71% change in apoptosis.

Table 3.4 - Annexin V Data

**C6 Annexin V**

| | Percent Apoptosis | | | Mean | Standard Error | Cell Viability | P-Value |
|---|---|---|---|---|---|---|---|
| | Trial 1 | Trial 2 | Trial 3 | | | | |
| Control | 10.3 | 6.3 | 10.7 | 9.10 | 1.09 | 90.90 | |
| QCT | 31.9 | 28.1 | 36.5 | 32.17 | 2.97 | 67.83 | 0.0002 |
| NaB | 22.4 | 21.2 | 22.4 | 22.00 | 0.35 | 78.00 | 0.0062 |
| QCT + NaB | 32.6 | 46.7 | 39.2 | 39.50 | 3.53 | 60.50 | < 0.0001 |

**T98G Annexin V**

| | Percent Apoptosis | | | Mean | Standard Error | Cell Viability | P-Value |
|---|---|---|---|---|---|---|---|
| | Trial 1 | Trial 2 | Trial 3 | | | | |
| Control | 11.3 | 10.4 | 9.3 | 10.33 | 0.58 | 89.67 | |
| QCT | 31.5 | 33.6 | 43.3 | 36.13 | 3.63 | 63.87 | < 0.0001 |
| NaB | 25.9 | 32.3 | 27.8 | 28.67 | 1.90 | 71.33 | 0.0002 |
| QCT + NaB | 42.8 | 43.8 | 42.6 | 43.07 | 0.37 | 56.93 | < 0.0001 |

**LN18 Annexin V**

| | Percent Apoptosis | | | Mean | Standard Error | Cell Viability | P-Value |
|---|---|---|---|---|---|---|---|
| | Trial 1 | Trial 2 | Trial 3 | | | | |
| Control | 11.6 | 8.1 | 9.7 | 9.80 | 1.01 | 90.20 | |
| QCT | 31.1 | 31.5 | 34.1 | 32.23 | 0.94 | 67.77 | < 0.0001 |
| NaB | 23.3 | 22.7 | 24.9 | 23.63 | 0.66 | 76.37 | < 0.0001 |
| QCT + NaB | 33.4 | 38.8 | 32.5 | 34.90 | 1.97 | 65.10 | < 0.0001 |

Table 3.4: This shows the data table for C6, T98G, and LN18 Annexin V trials. Standard error was calculated with the equation [Standard Error = StDev/Sqrt(3)]. Cell viability was calculated with the equation [Viability % = 100-MeanApoptosis]. P-values were calculated using the Minitab Express software with a one-way ANOVA followed by a Fisher post-hoc test.

Despite Annexin V being a well accepted test for the quantification of apoptosis, it is not without its downfalls. The greatest downfall for this test is the possibility of mechanical damage when preparing samples. T98G is the best example for mechanical damage possibly altering results. The human GBM cell lines T98G and LN18 are significantly more adhesive than the rat cell line C6. The cells are also much larger, as seen with Wright Staining. Due to the greater adhesive properties of the GBM human cell lines, vigorous cell scraping along with longer trypsinization times were used to harvest a satisfactory number of cells to be measured on the flow cytometer.

**Acridine Orange**

Acridine orange staining was used to visualize and quantify the total amount of acidic vesicular organelles (AVOs) in a cell population. It has been widely proven that the quantitiy of AVOs directly correlates to the amount of cells undergoing autophagy. Therefore, in order to visualize autophagy progression, AO staining was performed viewed via flow cytometry and flourescent microscopy.

Control and NaB images demonstrate how the small acidic lysosomes become widely distributed throughout the cell; in some cases completely englufing the cell body (as seen in T98G). Since QCT and QCT + NaB samples showed almost a complete inhibition of autophagy, the AO-stained images are able to show the distribution of acidic lysosomes as seen in a normally functioning cell. The autophagy inhibited cells are seen to have several small acidic lysosomes spread throughout the cell that play a role in routine cellular maintenance.

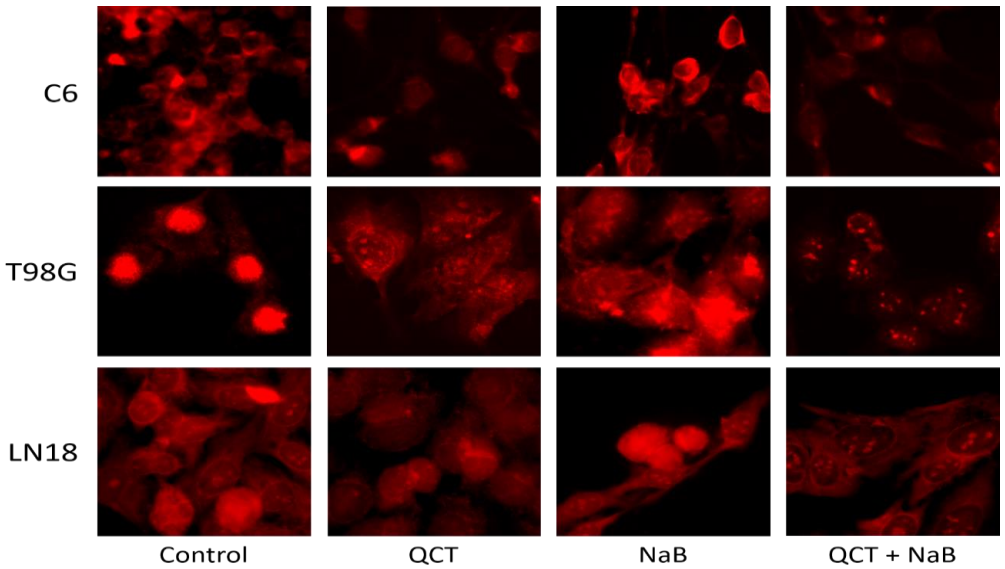


Figure 3.18: Acridine orange staining on C6, T98G, and LN18 cells shows acidic vesicular organelles engulf a cell undergoing autophagy. Bright red flourescence indicates an AVO. All images were taken at 40X magnification on a LeicaDM 2500 fluorescent microscope with a Texas Red filter.

C6 and T98G acridine orange stained samples were run through a flow cytometer to quantify the amount of light emission in the FL-3 channel, which directly correlates to the amount of autophagic cells in a population. The results showed a 25-30% increase in autophagy within 12 hours of serum starvation. C6 and T98G cells appeared to have the greatest amount of autophagy after 24 hours of serum starvation. After 48 hours of serum starvation, the total FL-3 density in C6 and T98G cell lines began to diminish. This could be due to be beginning of autophagy-induced cell death, which may also account for the 6-10% apoptosis seen in Annexin V & Wright Staining control samples.

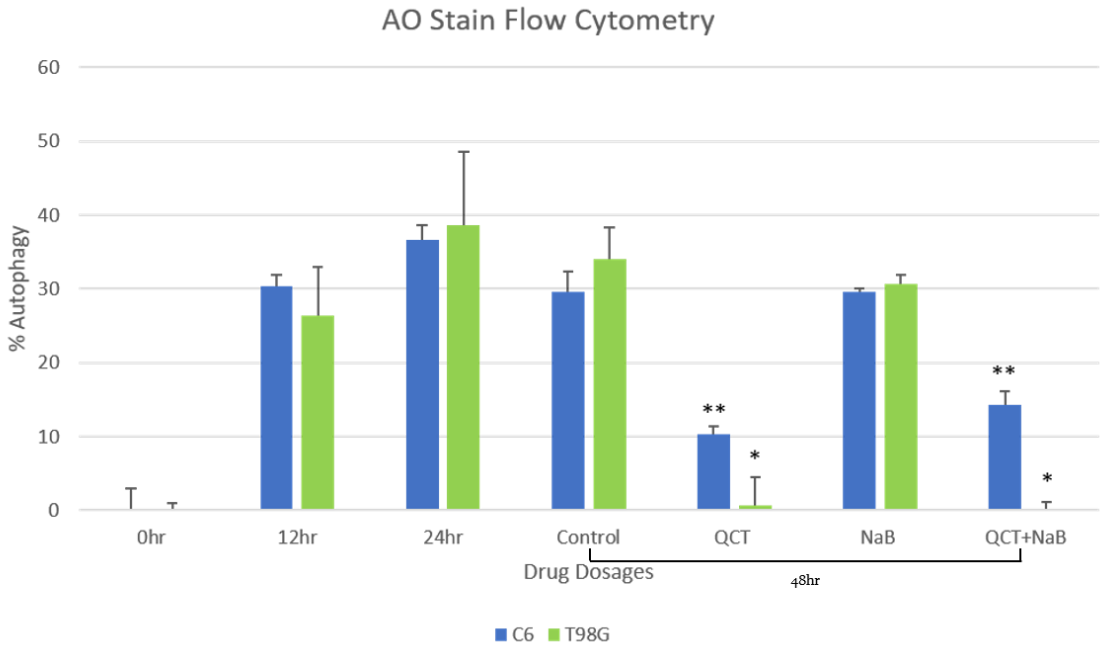


$* p < 0.05, ** p < 0.0001$

Figure 3.19: A graphical representation of autophagy expression measured by FL-3 density on a Cytomics FC500 Flow Cytometer. All samples are normalized to a 0 hr autophagy of 0%. All statistics were calculated on Minitab Express software.

After 24 hours of QCT, NaB, and QCT + NaB treatment, changes in autophagy expression began to occur. QCT-only samples showed a drastic reduction in autophagy levels in both C6 and T98G cell lines, with the greatest reduction occurring in T98G. NaB showed that it has very little impact on autophagy expression in both cell lines. QCT + NaB samples showed a synergistic effect on autophagy reduction in T98G cells, but showed slight antagonism in C6 cells. This result may explain why T98G has greater amounts of apoptosis in QCT + NaB combinations than C6 and LN18 cell lines. Since QCT + NaB is reducing protective autophagy, T98G cells may be more susceptible to treatment.

Table 3.5 - Acridine Orange Stain Data

**C6 AO Stain**

| | FL-3 Quantification | | | Mean | Normalized | Standard Error | P-value |
|---|---|---|---|---|---|---|---|
| | Trial 1 | Trial 2 | Trial 3 | | | | |
| 0hr | 60 | 70 | 67 | 65.67 | 0.00 | 2.96 | |
| 12hr | 98 | 93 | 97 | 96.00 | 30.33 | 1.53 | |
| 24hr | 102 | 99 | 106 | 102.33 | 36.67 | 2.03 | |
| Control | 90 | 98 | 98 | 95.33 | 29.67 | 2.67 | |
| Q25 | 75 | 78 | 75 | 76.00 | 10.33 | 1.00 | <0.0001 |
| B1 | 95 | 96 | 95 | 95.33 | 29.67 | 0.33 | 1 |
| Q25B1 | 77 | 80 | 83 | 80.00 | 14.33 | 1.73 | <0.0001 |

**T98G AO Stain**

| | FL-3 Quantification | | | Mean | Normalized | Standard Error | P-value |
|---|---|---|---|---|---|---|---|
| | Trial 1 | Trial 2 | Trial 3 | | | | |
| 0hr | 44 | 47 | 44 | 45.00 | 0.00 | 1.00 | |
| 12hr | 82 | 59 | 73 | 71.33 | 26.33 | 6.69 | |
| 24hr | 64 | 93 | 94 | 83.67 | 38.67 | 9.84 | |
| Control | 72 | 78 | 87 | 79.00 | 34.00 | 4.36 | |
| QCT | 53 | 40 | 44 | 45.67 | 0.67 | 3.84 | 0.0004 |
| NaB | 75 | 74 | 78 | 75.67 | 30.67 | 1.20 | 0.6484 |
| QCT+NaB | 45 | 43 | 47 | 45.00 | 0.00 | 1.15 | 0.0003 |

Table 3.5: Data tables showing C6 and T98G AO stain flow cytometry data. All samples were normalized to the non-serum starved 0 hr samples. Standard error was calculated using the equation: *Stdev(Trials1-3)/Sqrt(3)*. P-values were calculated using a one-way ANOVA and Fisher post-hoc test in the Minitab Express software.

## Western Blot

Western blotting was performed on C6 GBM cell lines and showed a detailed mechanism into how QCT, NaB, and QCT + NaB promote apoptosis. All samples were prepared using the previously outlined experimental protocol. Based off the previously mentioned experiments, QCT is the primary inducer of apoptosis with NaB supplementing its effects. As mentioned in *Taylor and Ray, 2017*, QCT acts primarily through activation of Caspase-3, 9, and increasing the Bax:Bcl-2 ratio. In addition to those apoptotic markers, PARP and survivin were also measured. PARP is a nuclear protein that contributes to many cellular processes including DNA repair, cell division, and apoptosis regulation (Zmuda et al., 2015). Survivin is a well-known apoptosis inhibitor that is highly upregulated in many forms of cancer, including GBM (Garg et al., 2016). A visualization of these proteins would provide a basic understanding of how QCT and NaB interact with each other to induce apoptosis.

Bcl-2 family genes are crucial for the regulation of apoptosis. This family consists of both pro- and anti-apoptotic genes that contribute to apoptosis through a variety of mechanisms, namely the intrinsic apoptosis pathway (Asmarinah et al., 2014). Bcl-2 is an anti-apoptotic protein that is located on the mitochondrial membrane and endoplasmic reticulum (Tsujimoto, 1998). Bcl-2 prevents apoptosis by preventing the release of cytochrome c and apoptosis inducing factor (AIF) from the mitochondrial membrane; thereby preventing the activation of the various caspases necessary for apoptosis induction. Many studies have shown that Bcl-2 upregulation can lead to chemo- and radioresistance in many cancers, including GBM. This makes Bcl-2 inhibitors a promising target for cancer therapy development.

Bax is a pro-apoptotic member of the Bcl-2 family. Within the intrinsic apoptotic pathway, mitochondrial outer membrane permeabilization is considered the point of no return. To arrive at this point, pro-caspase 8 is cleaved into caspase-8 which then cleaves BID → tBID. Promotion by tBID allows Bax to attach onto the outer mitochondrial membrane and forms pores, which then allows cytochrome C to exit the mitochondria and continue down the intrinsic mitochondrial pathway (Raemy and Martinou, 2014). Bax, along with Bak are directly responsible for mitochondrial permeabilization; thus, the furthering apoptosis.

Many studies have shown that comparing a tumor's Bax:Bcl-2 ratio can provide insight into how susceptible a tumor may be to chemo-/radio-resistance and how easily it may be treated (Mohammadian et al., 2016). High levels of intracellular Bax along with low levels of intracellular Bcl-2 can make a cell more apt to react to apoptotic stimuli; whereas the reverse can induce resistance to treatment and assist in tumor progression. Upregulation of STAT3, a human transcription activator, is able to increase Bcl-2 expression (Mohammadian et al., 2016). However, it has been documented that QCT downregulates JAK1 in glioblastoma, which is the upstream activator of STAT3 (Taylor & Ray, 2017). This leads to the hypothesis that QCT has the potential to lower Bcl-2 levels in both the single QCT samples and dual QCT + NaB samples.

This study showed evidence that QCT in combination with NaB increased the Bax:Bcl-2 ratio. This means that the intrinsic apoptotic pathway is progressing due to the QCT + NaB treatment. In the QCT-only samples, Bcl-2 was greatly inhibited while levels of activated Bax stayed relatively the same. NaB-only samples had a slight increase in Bax but little inhibition of Bcl-2. It has been well documented that QCT acts

through the intrinsic apoptosis pathway in GBM. The results obtained in this study remain conflicting due to the relatively small changes occurring to Bax and Bcl-2 in QCT-only doses along with the increase in both Bax and Bcl-2 levels in QCT + NaB doses. More investigation into the mitochondrial apoptosis proteins must be done in order to adequately draw a conclusion on whether QCT & NaB act synergistically in altering the Bax:Bcl-2 ratio.

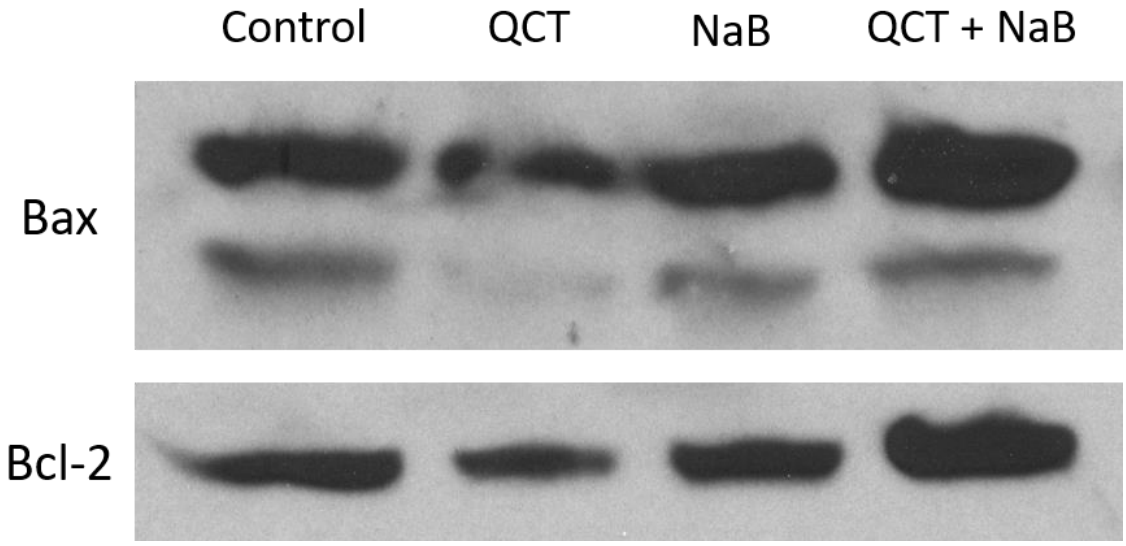


Figure 3.20: Western blotting of C6 cells treated in 48-hour serum starved conditions with either 25 µM QCT, 1 mM NaB, or QCT + NaB in combination. This blot shows both Bax (24 kD), cleaved Bax (21 kD), and Bcl-2 (26kD). Primary rabbit antibody was diluted 1:500 and the secondary HRP-conjugated antibody was diluted 1:10,000. Primary incubation took place overnight at 4°C and secondary incubation took place at RT for 30 minutes.

Caspases are a family of proteases that perform essential roles in the cell cycle and apoptosis. They act by performing a nucleophilic attack on aspartate residues on proteins; thus, performing proteolytic cleavage on the target proteins (Gervais et al., 1999). Caspase-3 may be one of the most widely studied caspase due to it being the primary executioner of apoptosis. After Bax acts on the mitochondria through the intrinsic apoptosis pathway, cytochrome C is released. Cytochrome C attaches to Apaf-1

in the cytosol, forming the apoptosome. The apoptosome then activates pro-caspase-9, an initiator caspase. This, in turn, activates effector caspases such as caspase-3. Caspase-3 can be activated by either the extrinsic pathway through caspase-8 or through the intrinsic pathway through caspase-9 (Reubold et al., 2011). Due to the crucial role of caspase-3 in apoptosis, many studies use the measurement of caspase-3 to analyze apoptotic cells in a population. This study is measuring both pro-caspase-3 (inactive) and cleaved caspase-3 (active) to determine how much apoptosis is being induced by each drug treatment.

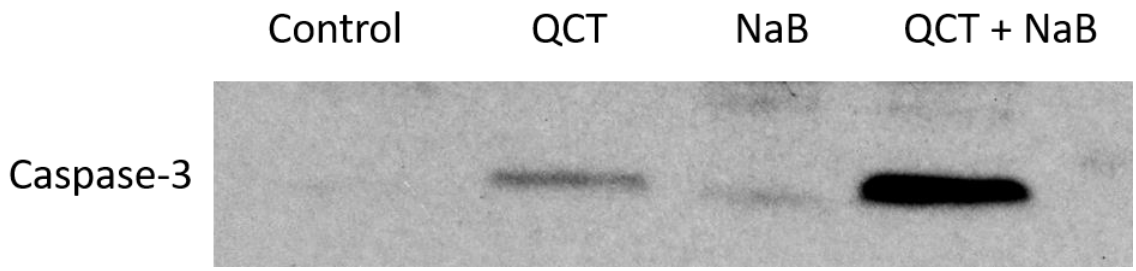


Figure 3.21: Western blotting of C6 cells treated in 48-hour serum starved conditions with either 25 µM QCT, 1 mM NaB, or QCT + NaB in combination. This blot shows cleaved caspase-3 (active). Primary rabbit antibody was diluted 1:1000 and the secondary HRP-conjugated antibody was diluted 1:10,000. Primary incubation took place overnight at 4°C and secondary incubation took place at RT for 30 minutes.

C6 control samples show almost no cleavage of caspase-3, meaning little-to-no apoptosis is occurring. QCT-only samples have a slight increase in apoptosis, which can be seen by the lower amounts of pro-caspase-3 and a band appearing for cleaved caspase-3. NaB-only samples do not have much activation of caspase-3, but a slight of cleaved caspase-3 can be seen forming. The most interesting aspect is the clear synergistic increase of cleaved caspase-3 in the QCT + NaB samples. This demonstrates that QCT and NaB are acting in synergism to promote higher amounts of apoptosis than QCT alone.

PARP is a protein residing in the nucleus that is responsible for ADP-ribosylation, which mediates a plethora of cellular processes including repair of single-stranded DNA breaks, cell division, and apoptosis regulation (Zmuda et al., 2015). In general, PARP is associated with continued cell survival. Because of this, PARP inhibition has been a widely-studied avenue for cancer therapy. The goal of PARP inhibition is to allow cancer cells to become more susceptible to DNA damaging chemotherapeutic agents, such as temozolomide (Zhu et al., 2015). PARP is inhibited through proteolytic cleavage, namely by the caspase proteins. It has been shown that almost all known caspases cleave PARP in some way. Cleavage of PARP is one of the most fundamental aspects of apoptosis (Chaitanya et al., 2010).

This study is aims to compare the activation of caspase-3 with the inactivation of PARP. The data collected on C6 shows a normal level of PARP activation in the control, QCT, and NaB samples. Despite the slight activation of caspase-3 by the single-dosed drugs, neither drug by itself was able to adequately inhibit PARP in any meaningful fashion. However, C6 cells treated with QCT + NaB showed a significant decrease in active PARP. This is another example of how QCT and NaB are profoundly synergistic with each other.

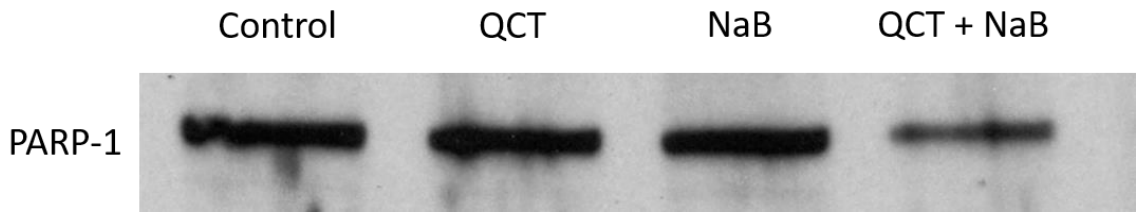


Figure 3.22: Western blotting of C6 cells treated in 48-hour serum starved conditions with either 25 µM QCT, 1 mM NaB, or QCT + NaB in combination. This blot shows active PARP-1. Primary rabbit antibody was diluted 1:1000 and the secondary HRP-conjugated antibody was diluted 1:10,000. Primary incubation took place overnight at 4°C and secondary incubation took place at RT for 30 minutes.

The impact of the QCT + NaB inhibition of PARP opens the door for many anti-cancer treatment avenues to be explored. Since PARP is a crucial DNA repair protein, downregulation can potentially hinder the resistance of GBM to many DNA damaging agents in-vivo. As previously mentioned in chapter 1, GBM becomes resistant to TMZ (a DNA alkylating agent) within about 15 months due to $O^6$-methylguanine DNA methyltransferase repairing the resulting DNA damage caused by treatment (Taylor & Ray 2017). Zhu et al. has suggested that PARP upregulation found in GBM is a major contributor to TMZ desensitization over time. By using QCT and NaB in conjunction with TMZ, GBM chemoresistance can be slowed; thus, allowing for a better prognosis in GBM patients.

Survivin is a member of the inhibitor of apoptosis (IAP) protein family. This family of proteins plays a major role in the regulation of apoptosis. The IAP family, along with survivin, includes XIAP, cIAP1, and Livin. Many speculate that increased survivin expression in cancer cells enables tumor progression through a variety of mechanisms (Gang et al., 2016). High survivin expression inhibits both the intrinsic and extrinsic apoptosis pathways by inhibiting caspase activation (Tamm et al., 1998). Direct binding of survivin to initiator and effector caspases is still being debated; however, survivin has been shown to bind directly to SMAC/DIABLO to prevent caspase activation (Garg et al., 2016). In addition to the inhibition of apoptosis, survivin has also been shown to upregulate VEGF expression in many cancer cells. VEGF is important in tumor angiogenesis because it enables nutrients to be provided to rapidly growing tumors

(Fernandez et al., 2014). These pro-tumor properties of survivin make it an ideal target for cancer therapy development.

This study showed a significant synergistic decrease in survivin expression with QCT and NaB combination. Control samples of C6 displayed a basal level of survivin expression, which is to be expected. QCT-only samples demonstrated that QCT by itself is a survivin inhibitor. But in all trials, QCT failed to completely inhibit all survivin expression. NaB-only samples showed that NaB is not a survivin inhibitor when acting alone. However, QCT + NaB in combination with each other showed almost a complete inhibition of survivin expression. QCT is inducing NaB to develop a property that is not typically seen when NaB is acting by itself. This demonstrates that QCT and NaB are working synergistically with each other to inhibit survivin expression.

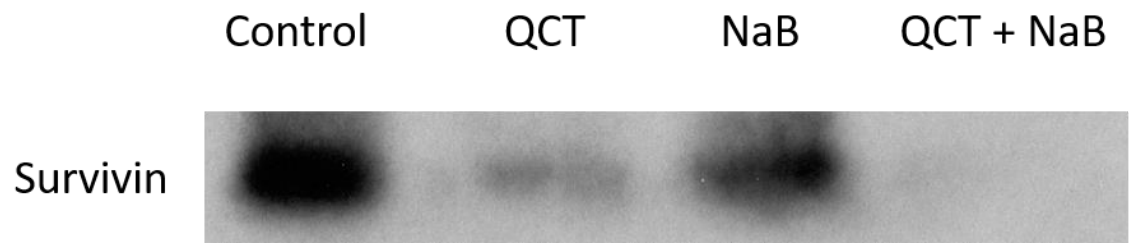


Figure 3.23: Western blotting of C6 cells treated in 48-hour serum starved conditions with either 25 µM QCT, 1 mM NaB, or QCT + NaB in combination. This blot shows active Survivin. Primary mouse antibody was diluted 1:1000 and the secondary HRP-conjugated antibody was diluted 1:10,000. Primary incubation took place overnight at 4°C and secondary incubation took place at RT for 30 minutes.

Many studies have been conducted on ways to inhibit survivin expression. Immunotherapies, small molecule inhibitors, and gene silencing are all methods being explored in an effort to downregulate survivin. Few studies have been conducted in GBM that explore the synergistic potential of survivin inhibition. A 2009 study demonstrated that QCT in combination with TRAIL induced survivin inhibition in GBM

cells at doses ranging from 100-200 µM (Siegelin et al., 2009). This study shows QCT is able to completely deplete survivin expression with 1/4$^{th}$ of the dose.

Another method for detecting levels of autophagy within a cell population is by measuring the protein LC3. LC3 (microtubule associated protein 1 light-chain 3) is part of the Atg (autophagy related) family of proteins, and is a crucial component for autophagy progression (Lee and Lee, 2016). As described in chapter 1, autophagy consists of the formation of an autophagosome that engulfs the cellular components destined for degradation. The autophagosome then fuses with an acidic lysosome and subsequently degrades the engulfed components; then to be reused as nutrients for the cell (Yang and Klionsky, 2010). Under normal growing conditions, LC3 resides mostly in the nucleus. Upon nutrient-deficient autophagy induction, LC3 becomes deacetylated by the deacetylase enzyme SIRT1 (Huang and Liu, 2015). LC3 then exits the nucleus and travels into the cytoplasm where LC3 becomes a required component to autophagosome formation and progression. In the cytoplasm, LC3 is cleaved by the protease ATG4(B) and then conjugated to Atg7, Atg3, and Atg12. This forms LC3-II, which is the form of LC3 bound to the autophagosome membrane. The amount of LC3-II directly correlates with the number of autophagosomes; thus, quantifying autophagy for a cell population (Lee and Lee, 2016).

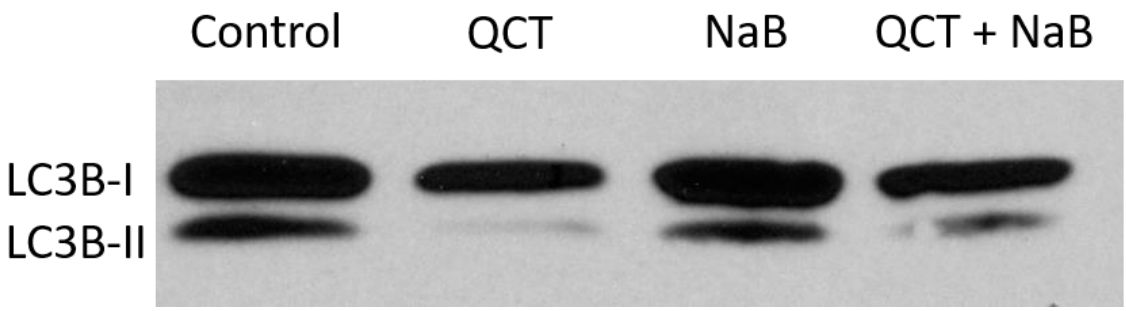


Figure 3.24: Western blotting of C6 cells treated in 48-hour serum starved conditions with either 25 µM QCT, 1 mM NaB, or QCT + NaB in combination. This blot shows LC3B-I (16 kD) and LC3B-II (14 kD). Primary rabbit antibody was diluted 1:1000 and the secondary HRP-conjugated antibody was diluted 1:10,000. Primary incubation took place overnight at 4°C and secondary incubation took place at RT for 30 minutes.

The shown results for C6 demonstrate that a significant amount of autophagy is occurring in the 48 hr serum-starved control samples, which is to be expected. QCT-only samples show a drastically decreased amount of autophagy, while NaB-only samples showed similar levels of autophagy compared to the control. This indicates that QCT is acting as an autophagy inhibitor while NaB has no impact on autophagy. QCT + NaB samples show a decreased amount of autophagy compared to the control but an increased amount compared to QCT-only samples. This indicates that NaB may be slightly hindering QCT's autophagy inhibition properties; however, the mechanism for this is unknown. The western blot data directly correlates with the AO stain data obtained via flow cytometry, which strengthens this conclusion.

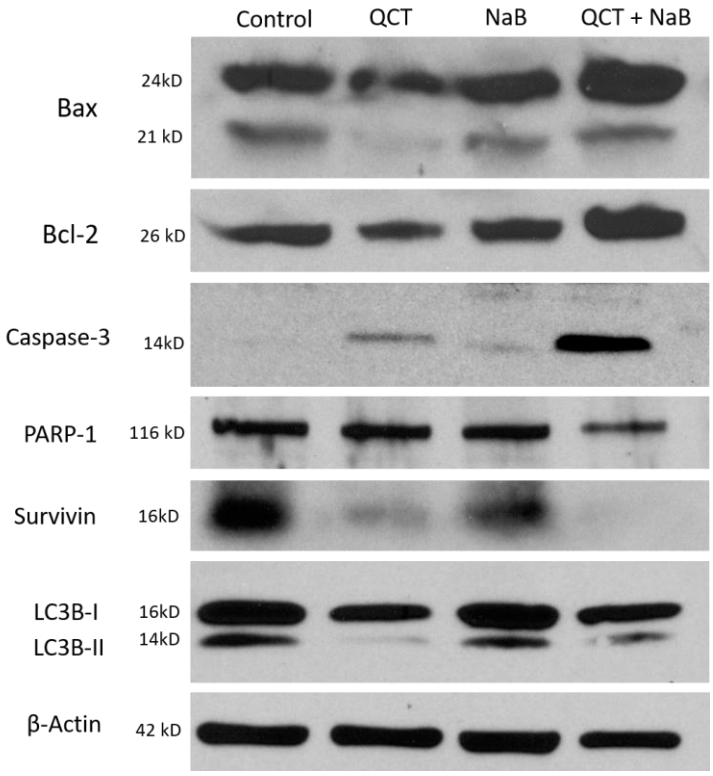


Figure 3.25: C6 GBM cell western blotting. All experiments were performed according to the previously described experimental protocol.

## 3.4 - FUTURE DIRECTIONS

### Nanocarrier Delivery

The synergistic data gathered on QCT + NaB combination therapy in glioblastoma points to the idea that quercetin has the potential to be a viable second-line glioblastoma therapy when combined with complementary drugs. But unfortunately, QCT has some downfalls that must be addressed before it can successfully be furthered into in-vivo studies. Quercetin is an abundant bioflavonoid that can be found in many common foods. But because QCT originates from food, the body has become very efficient at inducing its breakdown, making it largely incapable of being stored in tissues. For QCT to be used as an anti-cancer therapy, a delivery mechanism must be developed that enables QCT to evade metabolism and penetrate the blood brain barrier.

Most studies conducted about QCT brain delivery focus on the anti-oxidant property of QCT. However, much of this data can also be applied to QCT as an anti-cancer agent. A study conducted on intravenous administration of QCT-loaded nanosomes on newborn piglets demonstrated that QCT was delivered to the brain with a concentration of 3.64 nM 60 minutes after administration (Blasina et al., 2015). Although this concentration allows QCT to act as a neuroprotectant, its final concentration is not conducive for anti-cancer activity. Another study investigated the potential of QCT brain delivery using QCT-loaded nano lipidic carriers. They measured a QCT concentration in brain tissues of 68.3 nM 12 hours after administration (Kumar et al., 2016). But this concentration is still significantly lower than any µM concentration where QCT could exert anti-cancer properties. Recently, however, a study was performed using freeze-dried polymeric micelles to encapsulate quercetin to be used as an in-vivo glioma treatment in rats. They demonstrated that gastric administration of QCT-loaded micelles significantly increased the survival time and decreased tumor volume in glioma-infected rats. Median life expectancy was increased by 2-fold in treated rats compared to control specimens (Wang et al., 2016). These studies have shown that quercetin metabolism in the liver and exclusion by the blood brain barrier can be avoided with the use of lipid-based nanocarriers. In the future, more investigation must occur in the anti-cancer capabilities of QCT in-vivo.

**PARP Inhibition with Temozolomide**

One of the greatest hurdles medicine faces when treating GBM is the rapid chemoresistance that develops when undergoing temozolomide treatment. TMZ acts as a DNA alkylating agent that transfers a methyl group to DNA by forming an unstable

methyldiazonium cation at physiological pH. The addition of a methyl group at the $O^6$ guanine position is the source of TMZ cytotoxicity and results in glioblastoma cell death (Messaoudi et al., 2015). Unfortunately, in about 15 months, many GBM patients become resistant to TMZ. This mostly occurs through the MGMT DNA repair enzyme. MGMT removes methyl groups from DNA by permanently attaching itself to the methyl group, prompting inactivation and degradation by a proteasome (Messaoudi et al., 2015). In order to combat TMZ resistance in GBM, drug synergism remains one of the most promising options. Many clinical trials are underway with hopes of combating MGMT-induced GBM chemoresistance, however most have had little success. A 2014 trial investigated the benefit of combining Cilengitide with standard TMZ treatment in glioblastoma patients and found minimal benefit to overall survival (Stupp et al., 2014). Many more clinical trials have been conducted aiming to combat TMZ resistance with few promising results (Messaoudi et al., 2015).

Another available strategy for inhibiting GBM TMZ resistance is PARP inhibition. PARP is a protein that plays a crucial role in the DNA base excision repair (BER) system, which is activated by DNA damage caused by agents such as TMZ (Messaoudi et al., 2015). Many studies have suggested that introducing a PARP inhibitor to routine GBM treatment may re-sensitize tumors to treatment. For example, a 2017 study studied the impact that Veliparib, a potent PARP inhibitor, had on GBM cell lines taken from patients who had already undergone standard GBM treatment and had subsequently become resistant. Their in-vivo results obtained from nude mice showed that a PARP inhibitor combined with radiation therapy improved survival times by 12-22% (Jue et al., 2017).

Our results showed that QCT in combination with NaB acted as a potent PARP inhibitor in serum-starved C6 rat glioma cells. A potential avenue to be explored could be with PARP combination treatment as a precursor to TMZ. This could promote downregulation of survivin and PARP to allow enhanced TMZ sensitivity.

## 3.5 - CONCLUSION

This study investigated the synergistic efficacy of quercetin and sodium butyrate in glioblastoma. The results showed morphological signs of apoptosis that included membrane blebbing, cell shrinkage, and chromatin condensation. Additional apoptosis quantification with Annexin V/PI staining showed a marked increase in apoptosis with QCT + NaB combination compared to single-dosed drugs in C6, T98G, and LN18 glioblastoma cell lines. The highest amount of apoptosis was found in the T98G glioblastoma cell line at approximately 43%. Similar amounts of apoptosis are typically seen in GBM cells treated with a single dose of QCT at 100 µM (Kim et al., 2013). These results support the idea that QCT in combination with synergistic compounds, such as NaB, produce similar anti-cancer effects at drastically lower concentrations. This approach has the potential to overcome the ongoing issue of delivering QCT to brain tissues at high enough concentrations to enable its anti-cancer effects as opposed to its anti-inflammatory neuroprotective effects. By lowering the QCT anti-cancer concentration threshold, lipid-based nanocarriers may soon be developed to enable quercetin to be a viable glioblastoma treatment.

Acridine orange staining by fluorescence microscopy and flow cytometry was used to measure and quantify autophagy in serum-starved GBM cells. Flow cytometry

results showed that QCT was a powerful autophagy inhibitor in all GBM cell lines, but showed the greatest impact in the T98G cell population. QCT and QCT + NaB samples showed a complete reversal of autophagy in T98G cells. The findings in T98G contradict the findings of Badziul et al. saying that QCT alone is a weak autophagy inducer in T98G cells. Western blot analysis of LC3B in C6 cells showed QCT-induced autophagy inhibition with slight antagonism in QCT + NaB samples. This data was confirmed with AO staining. QCT as an autophagy inhibitor opens the door for enhanced glioblastoma treatment by reducing protective autophagy.

Western blotting in C6 showed synergism in caspase-3 activation, survivin inhibition, and PARP inhibition. Caspase-3, being one of the hallmarks of apoptosis, further demonstrates the synergistic effects of QCT and NaB on apoptosis induction. Survivin inhibition was obtained at drastically lower than previously seen concentrations in other quercetin combination studies (Siegelin et al., 2009). PARP inhibition caused by synergistic interactions between QCT and NaB shows the potential for this therapy to sensitize TMZ resistant cells for further treatments.

Overall, quercetin has been shown to be a powerful anti-cancer agent in glioblastoma. Despite the hurdles faced with quercetin-based treatment development, promising avenues have emerged. Quercetin pairing with synergistic compounds, such as sodium butyrate, enables effective quercetin concentrations to be drastically lowered. Continued synergistic studies, along with the development of efficient nano-delivery systems, could make quercetin administration a viable treatment for glioblastoma patients and give them a better chance at defeating this devastating disease.

# REFERENCES


Asmarinah, Paradowska-Dogan, A., Kodariah, R., Tanuhardja, B., Waliszewski, P., Mochtar, C. A., … Hinsch, E. (2014). Expression of the Bcl-2 family genes and complexes involved in the mitochondrial transport in prostate cancer cells. *International Journal of Oncology*, *45*(4), 1489–1496. http://doi.org/10.3892/ijo.2014.2576

Badalà, F., Nouri-mahdavi, K., & Raoof, D. A. (2008). NIH Public Access. *Computer*, *144*(5), 724–732. http://doi.org/10.1038/jid.2014.371

Bądziul, D., Jakubowicz-Gil, J., Langner, E., Rzeski, W., Głowniak, K., & Gawron, A. (2014). The effect of quercetin and imperatorin on programmed cell death induction in T98G cells in vitro. *Pharmacological Reports*, *66*(2), 292–300. http://doi.org/10.1016/j.pharep.2013.10.003

Berni Canani, R., Di Costanzo, M., & Leone, L. (2012). The epigenetic effects of butyrate: potential therapeutic implications for clinical practice. *Clinical Epigenetics*, *4*(1), 4. http://doi.org/10.1186/1868-7083-4-4

Birner, P., Toumangelova-Uzeir, K., Natchev, S., & Guentchev, M. (2010). STAT3 tyrosine phosphorylation influences survival in glioblastoma. *Journal of Neuro-Oncology*, *100*(3), 339–343. http://doi.org/10.1007/s11060-010-0195-8

Blasina, F., Vaamonde, L., Silvera, F., Tedesco, A. C., & Dajas, F. (2015). Intravenous nanosomes of quercetin improve brain function and hemodynamic instability after severe hypoxia in newborn piglets. *Neurochemistry International*, *89*, 149–156. http://doi.org/10.1016/j.neuint.2015.08.007

Boulares, A. H., Yakovlev, A. G., Ivanova, V., Stoica, B. A., Wang, G., Iyer, S., … Chem, M. J. B. (1999). Role of Poly ( ADP-ribose ) Polymerase ( PARP ) Cleavage in Apoptosis, *274*(33), 22932–22940. http://doi.org/10.1074/jbc.274.33.22932

Chaitanya, G. V, Steven, A. J., & Babu, P. P. (2010). PARP-1 cleavage fragments: signatures of cell-death proteases in neurodegeneration. *Cell Commun Signal*, *8*(1), 31. http://doi.org/10.1186/1478-811X-8-31

Chakrabarti, A., Oehme, I., Witt, O., Oliveira, G., Sippl, W., Romier, C., … Jung, M. (2015). HDAC8: A multifaceted target for therapeutic interventions. *Trends in*

*Pharmacological Sciences*, *36*(7), 481–492. http://doi.org/10.1016/j.tips.2015.04.013

Chen, B. L., Wang, L. T., Huang, K. H., Wang, C. C., Chiang, C. K., & Liu, S. H. (2014). Quercetin attenuates renal ischemia/reperfusion injury via an activation of AMP-activated protein kinase-regulated autophagy pathway. *Journal of Nutritional Biochemistry*, *25*(11), 1226–1234. http://doi.org/10.1016/j.jnutbio.2014.05.013

Chou, T. C. (2010). Drug combination studies and their synergy quantification using the chou-talalay method. *Cancer Research*, *70*(2), 440–446. http://doi.org/10.1158/0008-5472.CAN-09-1947

Cooper, S. T., & McNeil, P. L. (2015). Membrane Repair: Mechanisms and Pathophysiology. *Physiological Reviews*, *95*(4), 1205–40. http://doi.org/10.1152/physrev.00037.2014

Cui, X., Luo, Y., Li, C., Li, Y., & Wang, Z. (2015). Changes of intracellular Ca2+ in quercetin-induced autophagy progression. *Acta Biochimica et Biophysica Sinica*, *47*(11), 908–914. http://doi.org/10.1093/abbs/gmv096

Dajas, F., Abin-Carriquiry, J. A., Arredondo, F., Blasina, F., Echeverry, C., Martínez, M., … Vaamonde, L. (2015). Quercetin in brain diseases: Potential and limits. *Neurochemistry International*, *89*, 140–148. http://doi.org/10.1016/j.neuint.2015.07.002

DAMASKOS, C., VALSAMI, S., KONTOS, M., SPARTALIS, E., KALAMPOKAS, T., KALAMPOKAS, E., … DIMITROULIS, D. (2017). Histone Deacetylase Inhibitors: An Attractive Therapeutic Strategy Against Breast Cancer. *Anticancer Research*, *37*(1), 35–46. http://doi.org/10.21873/anticanres.11286

de Boer, V. C. J., Dihal, A. a, van der Woude, H., Arts, I. C. W., Wolffram, S., Alink, G. M., … Hollman, P. C. H. (2005). Tissue distribution of quercetin in rats and pigs. *The Journal of Nutrition*, *135*(7), 1718–1725. http://doi.org/135/7/1718

Eroglu, C. (2009). The role of astrocyte-secreted matricellular proteins in central nervous system development and function. *Journal of Cell Communication and Signaling*, *3*(3–4), 167–176. http://doi.org/10.1007/s12079-009-0078-y

Fernández, J. G., Rodríguez, D. A., Valenzuela, M., Calderon, C., Urzúa, U., Munroe, D., … Quest, A. F. (2014). Survivin expression promotes VEGF-induced tumor angiogenesis via PI3K/Akt enhanced β-catenin/Tcf-Lef dependent transcription. *Molecular Cancer*, *13*(1), 209. http://doi.org/10.1186/1476-4598-13-209

Fresno Vara, J. A., Casado, E., de Castro, J., Cejas, P., Belda-Iniesta, C., & González-Barón, M. (2004). PI3K/Akt signalling pathway and cancer. *Cancer Treat Rev*, *30*(2), 193–204. http://doi.org/10.1016/j.ctrv.2003.07.007

Gardi, C., Bauerova, K., Stringa, B., Kuncirova, V., Slovak, L., Ponist, S., … Russo, G. L. (2015). Quercetin reduced inflammation and increased antioxidant defense in rat adjuvant arthritis. *Archives of Biochemistry and Biophysics*, *583*, 150–157. http://doi.org/10.1016/j.abb.2015.08.008

Garg, H., Suri, P., Gupta, J. C., Talwar, G. P., & Dubey, S. (2016). Survivin: a unique target for tumor therapy. *Cancer Cell International*, *16*, 49. http://doi.org/10.1186/s12935-016-0326-1

Gervais, F. G., Xu, D., Robertson, G. S., Vaillancourt, J. P., Zhu, Y., Huang, J., … Nicholson, D. W. (1999). Involvement of caspases in proteolytic cleavage of Alzheimer's amyloid- ?? precursor protein and amyloidogenic A?? peptide formation. *Cell*, *97*(3), 395–406. http://doi.org/10.1016/S0092-8674(00)80748-5

Gibbons, J. (2014). Western Blot: Protein transfer overview. *North American Journal of Medical Sciences*, *6*(3), 158–159. http://doi.org/10.4103/1947-2714.128481

Glässer, G., Graefe, E. U., Struck, F., Veit, M., & Gebhardt, R. (2002). Comparison of antioxidative capacities and inhibitory effects on cholesterol biosynthesis of quercetin and potential metabolites. *Phytomedicine : International Journal of Phytotherapy and Phytopharmacology*, *9*(1), 33–40. http://doi.org/10.1078/0944-7113-00080

Golden, E. B., Cho, H.-Y., Jahanian, A., Hofman, F. M., Louie, S. G., Schönthal, A. H., & Chen, T. C. (2014). Chloroquine enhances temozolomide cytotoxicity in malignant gliomas by blocking autophagy. *Neurosurgical Focus*, *37*(6), E12. http://doi.org/10.3171/2014.9.FOCUS14504

Grande, F., Parisi, O. I., Mordocco, R. A., Rocca, C., Puoci, F., Scrivano, L., … Angelone, T. (2015). Quercetin derivatives as novel antihypertensive agents: Synthesis and physiological characterization. *European Journal of Pharmaceutical Sciences : Official Journal of the European Federation for Pharmaceutical Sciences*, *82*, 161–170. http://doi.org/10.1016/j.ejps.2015.11.021

Hingorani, R., Deng, J., Elia, J., McIntyre, C., & Mittar, D. (2011). Detection of Apoptosis Using the BD Annexin V FITC Assay on the BD FACSVerse™ System. *BD Biosciences*, *August*(August), 1–12. http://doi.org/10.1016/j.pestbp.2011.02.012.Investigations

Hong, D. S., Angelo, L. S., & Kurzrock, R. (2007). Interleukin-6 and its receptor in cancer: Implications for translational therapeutics. *Cancer*, *110*(9), 1911–1928. http://doi.org/10.1002/cncr.22999

Hottinger, A. F., Stupp, R., & Homicsko, K. (2014). Standards of care and novel approaches in the management of glioblastoma multiforme. *Chinese Journal of Cancer*, *33*(1), 32–39. http://doi.org/10.5732/cjc.013.10207

Huang, R., & Liu, W. (2015). Identifying an essential role of nuclear LC3 for autophagy. *Autophagy*, *11*(5), 852–853. http://doi.org/10.1080/15548627.2015.1038016

Ishisaka, A., Ichikawa, S., Sakakibara, H., Piskula, M. K., Nakamura, T., Kato, Y., … Terao, J. (2011). Accumulation of orally administered quercetin in brain tissue and its antioxidative effects in rats. *Free Radical Biology and Medicine*, *51*(7), 1329–1336. http://doi.org/10.1016/j.freeradbiomed.2011.06.017

Jakubowicz-Gil, J., Langner, E., Bądziul, D., Wertel, I., & Rzeski, W. (2013). Apoptosis induction in human glioblastoma multiforme T98G cells upon temozolomide and quercetin treatment. *Tumor Biology*, *34*(4), 2367–2378. http://doi.org/10.1007/s13277-013-0785-0

Jakubowicz-Gil, J., Langner, E., Bądziul, D., Wertel, I., & Rzeski, W. (2014). Quercetin and sorafenib as a novel and effective couple in programmed cell death induction in human gliomas. *Neurotoxicity Research*, *26*(1), 64–77. http://doi.org/10.1007/s12640-013-9452-x

Jang, B., Kwon, H., Katila, P., Lee, S. J., & Lee, H. (2016). Dual delivery of biological therapeutics for multimodal and synergistic cancer therapies. *Advanced Drug Delivery Reviews*, *98*, 113–133. http://doi.org/10.1016/j.addr.2015.10.023

Jhanji, V., Chan, E., Das, S., Zhang, H., & Vajpayee, R. B. (2011). Trypan blue dye for anterior segment surgeries. *Eye (London, England)*, *25*(9), 1113–20. http://doi.org/10.1038/eye.2011.139

Jue, T. R., Nozue, K., Lester, A. J., Joshi, S., Schroder, L. B. W., Whittaker, S. P., … McDonald, K. L. (2017). Veliparib in combination with radiotherapy for the treatment of MGMT unmethylated glioblastoma. *Journal of Translational Medicine*, *15*(1), 61. http://doi.org/10.1186/s12967-017-1164-1

Kashino, Y., Murota, K., Matsuda, N., Tomotake, M., Hamano, T., Mukai, R., & Terao, J. (2015). Effect of Processed Onions on the Plasma Concentration of Quercetin in Rats and Humans. *Journal of Food Science*, *80*(11), H2597–H2602. http://doi.org/10.1111/1750-3841.13079

Kiekow, C. J., Figueiró, F., Dietrich, F., Vechia, L. D., Pires, E. N. S., Jandrey, E. H. F., … Gosmann, G. (2016). Quercetin derivative induces cell death in glioma cells by modulating NF-??B nuclear translocation and caspase-3 activation. *European Journal of Pharmaceutical Sciences*, *84*, 116–122. http://doi.org/10.1016/j.ejps.2016.01.019

Kim, H., Moon, J. Y., Ahn, K. S., & Cho, S. K. (2013). Quercetin induces mitochondrial mediated apoptosis and protective autophagy in human glioblastoma U373MG Cells. *Oxidative Medicine and Cellular Longevity*, *2013*. http://doi.org/10.1155/2013/596496

Kloepper, J., Riedemann, L., Amoozgar, Z., Seano, G., Susek, K., Yu, V., … Jain, R. K. (2016). Ang-2/VEGF bispecific antibody reprograms macrophages and resident microglia to anti-tumor phenotype and prolongs glioblastoma survival. *Proceedings of the National Academy of Sciences of the United States of America*, *113*(16), 4476–81. http://doi.org/10.1073/pnas.1525360113

Konar, N. (2013). Non-isoflavone phytoestrogenic compound contents of various legumes. *European Food Research and Technology*, *236*(3), 523–530. http://doi.org/10.1007/s00217-013-1914-0

Kumar, P., Sharma, G., Kumar, R., Singh, B., Malik, R., Katare, O. P., & Raza, K. (2016). Promises of a biocompatible nanocarrier in improved brain delivery of quercetin: biochemical, pharmacokinetic and biodistribution evidences. *International Journal of Pharmaceutics*, *515*(1–2), 307–314. http://doi.org/10.1016/j.ijpharm.2016.10.024

Lauretti, F., Lucas De Melo, F., Benati, F. J., De Mello Volotão, E., Santos, N., Carvalho Linhares, R. E., & Nozawa, C. (2003). Use of acridine orange staining for the detection of rotavirus RNA in polyacrylamide gels. *Journal of Virological Methods*, *114*(1), 29–35. http://doi.org/10.1016/j.jviromet.2003.08.005

Lee, D. H., Ryu, H.-W., Won, H.-R., & Kwon, S. H. (2015). Advances in epigenetic glioblastoma therapy. *Oncotarget*. http://doi.org/10.18632/oncotarget.14612

Lee, Y. K., & Lee, J. A. (2016). Role of the mammalian ATG8/LC3 family in autophagy: Differential and compensatory roles in the spatiotemporal regulation of autophagy. *BMB Reports*, *49*(8), 424–430. http://doi.org/10.5483/BMBRep.2016.49.8.081

Li, J., Tang, C., Li, L., Li, R., & Fan, Y. (2016). Quercetin sensitizes glioblastoma to t-AUCB by dual inhibition of Hsp27 and COX-2 in vitro and in vivo. *Journal of Experimental & Clinical Cancer Research : CR*, *35*(1), 61. http://doi.org/10.1186/s13046-016-0331-1

Li, J., Tang, C., Li, L., Li, R., & Fan, Y. (2016). Quercetin blocks t-AUCB-induced autophagy by Hsp27 and Atg7 inhibition in glioblastoma cells in vitro. *Journal of Neuro-Oncology*, *129*(1), 39–45. http://doi.org/10.1007/s11060-016-2149-2

Liu, L., Tang, Y., Gao, C., Li, Y., Chen, S., Xiong, T., … Yao, P. (2014). Characterization and biodistribution in vivo of quercetin-loaded cationic nanostructured lipid carriers. *Colloids and Surfaces B: Biointerfaces*, *115*, 125–131. http://doi.org/10.1016/j.colsurfb.2013.11.029

Lotte, M. E., Berghauser, P., Jochem, K. H. S., Subramanian, V., Sigrid, S., Jenneke J, K., … Sieger, L. (2014). The Bcl-2 inhibitor Obatoclax overcomes resistance to histone deacetylase inhibitors SAHA and LBH589 as radiosensitizers in patient-

derived glioblastoma stem-like cells. *Genes & Cancer*, *5*(November), 445–459. http://doi.org/10.18632/genesandcancer.42

Lu, N. T., Crespi, C. M., Liu, N. M., Vu, J. Q., Ahmadieh, Y., Wu, S., … French, S. W. (2016). A Phase i Dose Escalation Study Demonstrates Quercetin Safety and Explores Potential for Bioflavonoid Antivirals in Patients with Chronic Hepatitis C. *Phytotherapy Research*, *30*(1), 160–168. http://doi.org/10.1002/ptr.5518

McIlwain, D. R., Berger, T., & Mak, T. W. (2015). Caspase Functions in Cell Death and Disease: Figure 1. *Cold Spring Harbor Perspectives in Biology*, *7*(4), a026716. http://doi.org/10.1101/cshperspect.a026716

Messaoudi, K., Clavreul, A., & Lagarce, F. (2015). Toward an effective strategy in glioblastoma treatment. Part I: resistance mechanisms and strategies to overcome resistance of glioblastoma to temozolomide. *Drug Discovery Today*, *20*(7), 899–905. http://doi.org/10.1016/j.drudis.2015.02.011

Michaud-Levesque, J., Bousquet-Gagnon, N., & Béliveau, R. (2012). Quercetin abrogates IL-6/STAT3 signaling and inhibits glioblastoma cell line growth and migration. *Experimental Cell Research*, *318*(8), 925–935. http://doi.org/10.1016/j.yexcr.2012.02.017

Mirzayans, R., Andrais, B., Kumar, P., & Murray, D. (2016). The Growing Complexity of Cancer Cell Response to DNA-Damaging Agents: Caspase 3 Mediates Cell Death or Survival? *International Journal of Molecular Sciences*, *17*(5), 708. http://doi.org/10.3390/ijms17050708

Mohammadian, J., Sabzichi, M., & Molavi, O. (2016). Combined Treatment with Stattic and Docetaxel Alters the Bax / Bcl-2 Gene Expression Ratio in Human Prostate Cancer Cells, *17*, 5031–5035. http://doi.org/10.22034/APJCP.2016.17.11.5031

Moon, J. H., Eo, S. K., Lee, J. H., & Park, S. Y. (2015). Quercetin-induced autophagy flux enhances TRAIL-mediated tumor cell death. *Oncology Reports*, *34*(1), 375–381. http://doi.org/10.3892/or.2015.3991

Murota, K., & Terao, J. (2003). Antioxidative flavonoid quercetin: Implication of its intestinal absorption and metabolism. *Archives of Biochemistry and Biophysics*, *417*(1), 12–17. http://doi.org/10.1016/S0003-9861(03)00284-4

Nugent, N. R. (2009). NIH Public Access. *American Journal Of Medical Genetics Part C Seminars In Medical Genetics*, *68*(2), 127–132. http://doi.org/10.1002/ajmg.c.30169.Genetics

Ohr, M. A. M., Rustrup, P. E. K., Ndersson, H. E. A., Irkendal, D. O. K., & Angsbo, J. E. N. S. B. (2008). Match a Ctivities of E Lite W Omen S Occer, *22*(2), 341–349.

Paller, C. J., Kanaan, Y. M., Beyene, D. A., Naab, T. J., Copeland, R. L., Tsai, H. L., … Hudson, T. S. (2015). Risk of prostate cancer in African-American men: Evidence of mixed effects of dietary quercetin by serum Vitamin D status. *Prostate*, *75*(13), 1376–1383. http://doi.org/10.1002/pros.23018

Pan, H.-C., Jiang, Q., Yu, Y., Mei, J.-P., Cui, Y.-K., & Zhao, W.-J. (2014). Quercetin promotes cell apoptosis and inhibits the expression of MMP-9 and fibronectin via the AKT and ERK signalling pathways in human glioma cells. *Neurochemistry International*, *80*, 60–71. http://doi.org/10.1016/j.neuint.2014.12.001

Pierzy??ska-Mach, A., Janowski, P. A., & Dobrucki, J. W. (2014). Evaluation of acridine orange, LysoTracker Red, and quinacrine as fluorescent probes for long-term tracking of acidic vesicles. *Cytometry Part A*, *85*(8), 729–737. http://doi.org/10.1002/cyto.a.22495

Pozsgai, E., Bellyei, S., Cseh, A., Boronkai, A., Racz, B., Szabo, A., … Hocsak, E. (2013). Quercetin Increases the Efficacy of Glioblastoma Treatment Compared to Standard Chemoradiotherapy by the Suppression of PI-3-Kinase-Akt Pathway. *Nutrition and Cancer*, *5581*(September), 37–41. http://doi.org/10.1080/01635581.2013.810291

Priprem, A., Watanatorn, J., Sutthiparinyanont, S., Phachonpai, W., & Muchimapura, S. (2008). Anxiety and cognitive effects of quercetin liposomes in rats. *Nanomedicine: Nanotechnology, Biology, and Medicine*, *4*(1), 70–78. http://doi.org/10.1016/j.nano.2007.12.001

Raemy, E., & Martinou, J. C. (2014). Involvement of cardiolipin in tBID-induced activation of BAX during apoptosis. *Chemistry and Physics of Lipids*, *179*, 70–74. http://doi.org/10.1016/j.chemphyslip.2013.12.002

Ravishankar, D., Rajora, A. K., Greco, F., & Osborn, H. M. I. (2013). Flavonoids as prospective compounds for anti-cancer therapy. *International Journal of Biochemistry and Cell Biology*, *45*(12), 2821–2831. http://doi.org/10.1016/j.biocel.2013.10.004Review

Reubold, T. F., Wohlgemuth, S., & Eschenburg, S. (2011). Crystal structure of full-length Apaf-1: How the death signal is relayed in the mitochondrial pathway of apoptosis. *Structure*, *19*(8), 1074–1083. http://doi.org/10.1016/j.str.2011.05.013

Sabogal-Guáqueta, A. M., Muñoz-Manco, J. I., Ramírez-Pineda, J. R., Lamprea-Rodriguez, M., Osorio, E., & Cardona-Gómez, G. P. (2015). The flavonoid quercetin ameliorates Alzheimer's disease pathology and protects cognitive and emotional function in aged triple transgenic Alzheimer's disease model mice. *Neuropharmacology*, *93*, 134–145. http://doi.org/10.1016/j.neuropharm.2015.01.027

Sang, D.-P., Li, R.-J., & Lan, Q. (2014). Quercetin sensitizes human glioblastoma cells to temozolomide in vitro via inhibition of Hsp27. *Acta Pharmacologica Sinica*, *35*(6), 832–8. http://doi.org/10.1038/aps.2014.22

Santos, B. L., Oliveira, M. N., Coelho, P. L. C., Pitanga, B. P. S., Da Silva, A. B., Adelita, T., … Costa, S. L. (2015). Flavonoids suppress human glioblastoma cell growth by inhibiting cell metabolism, migration, and by regulating extracellular matrix proteins and metalloproteinases expression. *Chemico-Biological Interactions*, *242*, 123–138. http://doi.org/10.1016/j.cbi.2015.07.014

Siegelin, M. D., Reuss, D. E., Habel, A., Rami, A., & von Deimling, A. (2009). Quercetin promotes degradation of survivin and thereby enhances death-receptor-mediated apoptosis in glioma cells. *Neuro-Oncology*, *11*(2), 122–31. http://doi.org/10.1215/15228517-2008-085

Skommer, J., Brittain, T., & Raychaudhuri, S. (2010). Bcl-2 inhibits apoptosis by increasing the time-to-death and intrinsic cell-to-cell variations in the mitochondrial pathway of cell death. *Apoptosis*, *15*(10), 1223–1233. http://doi.org/10.1007/s10495-010-0515-7

Strober, W. (2001). Trypan blue exclusion test of cell viability. *Current Protocols in Immunology / Edited by John E. Coligan ... [et Al.]*, *Appendix 3*, Appendix 3B. http://doi.org/10.1002/0471142735.ima03bs21

Stupp, R., Hegi, M. E., Gorlia, T., Erridge, S. C., Perry, J., Hong, Y. K., … Weller, M. (2014). Cilengitide combined with standard treatment for patients with newly diagnosed glioblastoma with methylated MGMT promoter (CENTRIC EORTC 26071-22072 study): a multicentre, randomised, open-label, phase 3 trial. *The Lancet. Oncology*, *15*(10), 1100–1108. http://doi.org/10.1016/S1470-2045(14)70379-1

Su, Q., Peng, M., Zhang, Y., Xu, W., Darko, K. O., Tao, T., … Yang, X. (2016). Quercetin induces bladder cancer cells apoptosis by activation of AMPK signaling pathway. *American Journal of Cancer Research*, *6*(2), 498–508.

Takayama, S., Reed, J. C., & Homma, S. (2003). Heat-shock proteins as regulators of apoptosis. *Oncogene*, *22*, 9041–9047. http://doi.org/10.1038/sj.onc.1207114

Tamm, I., Wang, Y., Sausville, E., Scudiero, D. A., Vigna, N., Oltersdorf, T., & Reed, J. C. (1998). IAP-family protein Survivin inhibits caspase activity and apoptosis induced by Fas (CD95), bax, caspases, and anticancer drugs. *Cancer Research*, *58*(23), 5315–5320.

Thomé, M. P., Filippi-Chiela, E. C., Villodre, E. S., Migliavaca, C. B., Onzi, G. R., Felipe, K. B., & Lenz, G. (2016). Ratiometric analysis of acridine orange staining in

the study of acidic organelles and autophagy. *Journal of Cell Science*, 4622–4632. http://doi.org/10.1242/jcs.195057

Tsujimoto, Y. (1998). Role of Bcl-2 family proteins in apoptosis: Apoptosomes or mitochondria? *Genes to Cells*, *3*(11), 697–707. http://doi.org/10.1046/j.1365-2443.1998.00223.x

Verhoven, B., Schlegel, R. A., & Williamson, P. (1995). Mechanisms of phosphatidylserine exposure, a phagocyte recognition signal, on apoptotic T lymphocytes. *Journal of Experimental Medicine*, *182*(5), 1597–1601. http://doi.org/10.1084/jem.182.5.1597

Wang, G., Wang, J. J., Chen, X. L., Du, L., & Li, F. (2016). Quercetin-loaded freeze-dried nanomicelles: Improving absorption and anti-glioma efficiency in vitro and in vivo. *Journal of Controlled Release*, *235*, 276–290. http://doi.org/10.1016/j.jconrel.2016.05.045

Wang, G., Wang, J., Luo, J., Wang, L., Chen, X., Zhang, L., & Jiang, S. (2013). PEG2000-DPSE-coated quercetin nanoparticles remarkably enhanced anticancer effects through induced programed cell death on C6 glioma cells. *Journal of Biomedical Materials Research - Part A*, *101*(11), 3076–3085. http://doi.org/10.1002/jbm.a.34607

Wang, Y., Xing, D., Zhao, M., Wang, J., & Yang, Y. (2016). The Role of a Single Angiogenesis Inhibitor in the Treatment of Recurrent Glioblastoma Multiforme: A Meta-Analysis and Systematic Review. *PLoS One*, *11*(3), e0152170. http://doi.org/10.1371/journal.pone.0152170

West, A. C., & Johnstone, R. W. (2014). New and emerging HDAC inhibitors for cancer treatment. *J Clin Invest.*, *124*(1), 30–39. http://doi.org/10.1172/JCI69738.30

Winkel-Shirley, B. (2001). Flavonoid biosynthesis. A colorful model for genetics, biochemistry, cell biology, and biotechnology. *Plant Physiology*, *126*(February 2015), 485–493. http://doi.org/10.1104/pp.126.2.485

Winkler, G. C., Barle, E. L., Galati, G., & Kluwe, W. M. (2014). Functional differentiation of cytotoxic cancer drugs and targeted cancer therapeutics. *Regulatory Toxicology and Pharmacology*, *70*(1), 46–53. http://doi.org/10.1016/j.yrtph.2014.06.012

Yang, Z., & Klionsky, D. J. (2010). Mammalian autophagy: Core molecular machinery and signaling regulation. *Current Opinion in Cell Biology*, *22*(2), 124–131. http://doi.org/10.1016/j.ceb.2009.11.014

Yin, N., Ma, W., Pei, J., Ouyang, Q., Tang, C., & Lai, L. (2014). Synergistic and antagonistic drug combinations depend on network topology. *PLoS ONE*, *9*(4). http://doi.org/10.1371/journal.pone.0093960

Yue, Q. F., Xiong, B., Chen, W. X., & Liu, X. Y. (2014). Comparative study of the efficacy of Wright-Giemsa stain and Liu's stain in the detection of Auer rods in acute promyelocytic leukemia. *Acta Histochemica*, *116*(6), 1113–1116. http://doi.org/10.1016/j.acthis.2014.05.005

Yurtsever, A., Haydaroglu, A., Biray Avci, C., Gunduz, C., Oktar, N., Dalbasti, T., … Kitapcioglu, G. (2013). Assessment of genetic markers and glioblastoma stem-like cells in activation of dendritic cells. *Human Cell*, *26*(3), 105–113. http://doi.org/10.1007/s13577-013-0065-8

Zamin, L. L., Filippi-Chiela, E. C., Vargas, J., Demartini, D. R., Meurer, L., Souza, A. P., … Lenz, G. (2014). Quercetin promotes glioma growth in a rat model. *Food and Chemical Toxicology : An International Journal Published for the British Industrial Biological Research Association*, *63*(2014), 205–11. http://doi.org/10.1016/j.fct.2013.11.002

Zhu, Q., Wang, X., Hu, Y., He, X., Gong, G., & Xu, Y. (2015). Discovery and SAR study of 2-(1-propylpiperidin-4-yl)-3H-imidazo[4,5-c]pyridine-7-carboxamide: A potent inhibitor of poly(ADP-ribose) polymerase-1 (PARP-1) for the treatment of cancer. *Bioorganic and Medicinal Chemistry*, *23*(20), 6551–6559. http://doi.org/10.1016/j.bmc.2015.09.026

Ziegler, U., & Groscurth, P. (2004). Morphological features of cell death. *Cardiovascular Research*, *19*(3), 124–128. http://doi.org/10.1152/nips.01519.2004

Zmuda, F., Malviya, G., Blair, A., Boyd, M., Chalmers, A. J., Sutherland, A., & Pimlott, S. L. (2015). Synthesis and evaluation of a radioiodinated tracer with specificity for poly(ADP-ribose) polymerase-1 (PARP-1) in vivo. *Journal of Medicinal Chemistry*, *58*(21), 8683–8693. http://doi.org/10.1021/acs.jmedchem.5b01324